Large Deviations of Reflected Diffusions

by

Johannes Petrus du Buisson

Thesis presented in partial fulfilment of the requirements for the degree of Master of Science (Theoretical Physics) in the Faculty of Science at Stellenbosch University

Supervisor: Prof. Hugo Touchette
Co-supervisor: Prof. Michael Kastner

March 2020

Declaration

By submitting this thesis electronically, I declare that the entirety of the work contained therein is my own, original work, that I am the sole author thereof (save to the extent explicitly otherwise stated), that reproduction and publication thereof by Stellenbosch University will not infringe any third party rights and that I have not previously in its entirety or in part submitted it for obtaining any qualification.

Date: March 2020

Abstract

Large Deviations of Reflected Diffusions

J.P du Buisson

Department of Physics,
University of Stellenbosch,
Stellenbosch, South Africa.

Thesis: MSc (Theoretical Physics)

March 2020

We study the fluctuations of time-integrated functionals of Markov diffusions evolving in a bounded domain. These fluctuations can be described in large deviation theory by the so-called rate function, which encodes information about the probability distribution of such functionals in the long-time limit. In practice, the rate function is obtained by performing a spectral calculation. Furthermore, solving the spectral problem allows us to construct an effective process which realizes a given fluctuation away from the mean and explains how that fluctuation is created dynamically in time. Most works in large deviation theory have considered Markov diffusions evolving in an unbounded domain (e.g. $\mathbb{R}$ or $\mathbb{R}^d$). In this thesis we consider diffusions in *bounded* domains with perfect reflection at the boundaries. Considering the one-dimensional case, we derive the appropriate boundary conditions on the spectral problem and explore the implications for the effective process. We apply this knowledge to obtain the rate function of the area of the reflected Ornstein-Uhlenbeck process and reflected Brownian motion with drift, and to obtain their effective process. A variational representation of the rate function is used to construct accurate approximations of the effective process for both of the systems considered.

Uittreksel

Groot Afwykings van Gereflekteerde Diffusies

("Large Deviations of Reflected Diffusions")

J.P du Buisson

Departement Fisika,
Universiteit van Stellenbosch,
Stellenbosch, Suid-Afrika.

Tesis: MSc (Theoretical Physics)

Maart 2020

Ons bestudeer die fluktuasies van tyd-geïntegreerde funksionale van Markov diffusies wat in 'n begrensde domein ewolueer. Hierdie fluktuasies kan in die teorie van groot afwykings deur die so-genoemde koers funksie, wat informasie rakende die waarskynlikheidsverspreiding van sulke funksionale in die lang-tyd limiet bevat, beskryf word. In die praktyk kan die koers funksie bepaal word deur 'n spektrale berekening uit te voer. Verder, die oplossing van die spektrale probleem stel ons daartoe in staat om 'n effektiewe proses te konstrueer, wat 'n gegewe fluksuasie weg van die gemiddeld realiseer en wat verduidelik hoe hierdie fluksuasie dinamies in tyd geskep word. Meeste navorsing in die teorie van groot afwykings handel met Markov diffusies wat in 'n onbegrensde domein (bv. $\mathbb{R}$ of $\mathbb{R}^d$) ewolueer. In hierdie tesis oorweeg ons diffusies in *begrensde* domeine met perfekte refleksie by die grense. Met betrekking tot die een-dimensionele geval, lei ons die gepaste grens toestande op die spektrale probleem af en ondersoek ons die implikasies vir die effektiewe proses. Ons pas hierdie kennis toe om die koers funksie vir die area van die gereflekteerde Ornstein-Uhlenbeck proses en gereflekteerde Browniese beweging met drif te bereken, en om hul effektiewe proses te bepaal. 'n Variationele verteenwoordiging van die koers funksie word gebruik om akkurate benaderings van die effektiewe proses vir beide van die stelses wat oorweeg is te konstrueer.

Acknowledgements

I would like to thank my supervisor, Hugo Touchette, for his guidance, support and patience. Without these things the completion of this thesis would have been impossible.

Words cannot express the gratitude I feel for everything my mother Annalise and father Dubbies have done for me, including their support over the course of this degree. Thank you.

Thank you to my sister Lise for our life-affirming conversations and for being the truly remarkable person that you are. The world would be a dull place without you.

Finally, I would like to thank my friends. In particular JC Louw, for many stimulating conversations regarding physics and life, and for being a source of emotional support, Riyaadh Jamodien for being someone to rely on and for providing a well-balanced and thoughtful perspective, Alex Leid for conversations ranging over a wide variety of topics and for being a fellow MSc SB, Taboka Prince Chalebgwa and Ignazio Ferreira for our intellectual discussions and for the interests that we share and Jason Harley for his remarkable generosity and erudition, and for supplying helpful advice and psychological insight.

Dedications

Dedicated to my family. L, A, D.

Contents

List of Figures

Chapter 1

Introduction

In this thesis we study the fluctuations of certain time-integrated functionals of Markov diffusions evolving in bounded domains. In particular, we will be concerned with understanding the fluctuations of such functionals away from their expected value in the long-time limit. In this chapter we describe the background relating to this topic as well as our motivation for studying it. We also provide an overview of our goals and contributions compared to the previous research done on the topics relating to the thesis, and give an outline of the structure of the thesis.

1.1 Brownian Motion

The phenomenon underlying the physical systems encountered in this thesis is Brownian motion, named after Robert Brown who, in 1827, studied the irregular motion of grains of pollen suspended in water. Brownian motion is illustrated in Fig. 1.1 (see [1] for information regarding the numerical simulation of Brownian motion). A probabilistic treatment of this form of motion as a Markov process in order to understand diffusion processes in physics, specifically the diffusion of suspended particles in a fluid, was initiated by Einstein [2]. Einstein's work was an important piece of evidence in support of the reality of atoms in that it allowed Avogadro's number N_A to be related to the mean square displacement of suspended particles, and thereby made the determination of Avogadro's number possible via experimental methods [3]. Such an experiment was conducted by Perrin and led to his being awarded the Nobel Prize in physics in 1926 [3]. The study of Brownian motion as a Markov process was also undertaken, independent of Einstein, by Smoluchowski [4].

Langevin [5] provided an alternative method of describing Brownian motion through the addition of a random force in Newton's equation of motion. Langevin's method forms the basis for the modern theory of stochastic differential equations, which was formalized and made rigorous by Itô, and is known as the Itô calculus [6]. A stochastic differential equation can be written in an

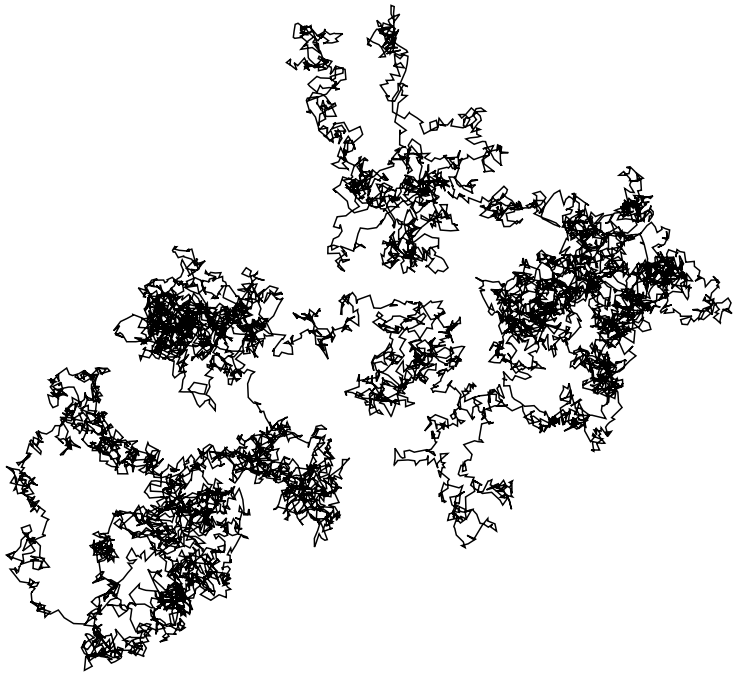

Figure 1.1: Sample path of Brownian motion in two dimensions.

informal manner as

$$\dot{X}_t = F(X_t) + \xi_t, \tag{1.1}$$

where the noise term ξ_t is taken to be the derivative of Brownian motion. In this manner, Brownian motion serves as a fundamental model of noise for continuous-time processes, called Gaussian white noise, accounting for external perturbations or uncertainty in the evolution of a system. As such, Brownian motion finds application in a large variety of instances, including:

- Non-equilibrium systems such as biomolecular motors and nano-machines in biophysics [7, 8]. The energetics of such machines are studied within the so-called theory of stochastic energetics [9].
- The manipulation of microscopic or mesoscopic systems immersed in a fluid such as the manipulation of a Brownian particle suspended in water via laser tweezers [10].
- The thermal current or voltage noise in electrical circuits. This type of noise is is known as Johnson-Nyquist noise.
- The measured intensity of a laser field in quantum optics [1].
- Dynamical systems perturbed by external noise sources, e.g., controlled systems with noisy inputs.
- Continuous limits of discrete-space systems, such as queues and biological populations [11].

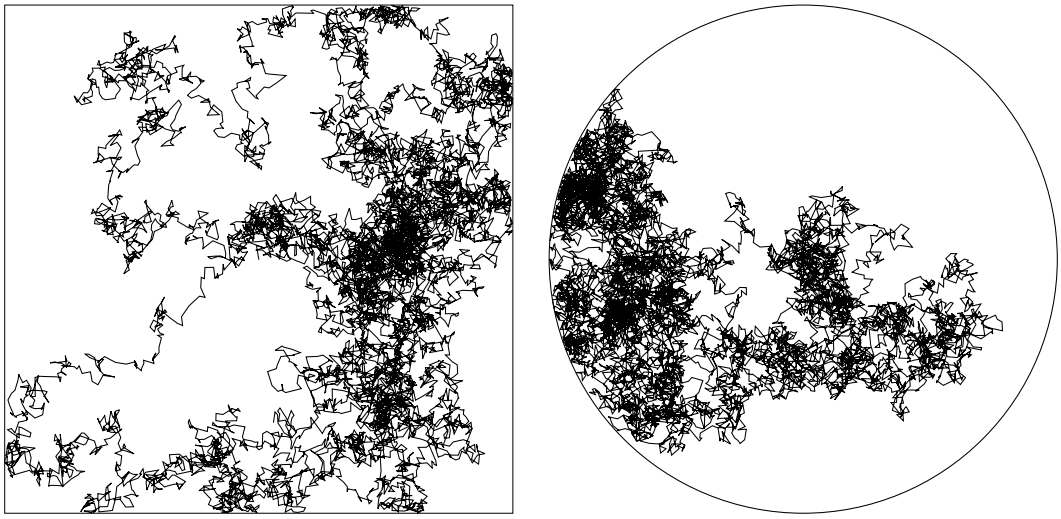

Figure 1.2: 2 Dimensional reflected Brownian motion shown for different boundary geometries. Left: Square domain. Right: Circular domain.

- In finance, where the evolution of stock prices is commonly modelled by the so-called geometric Brownian motion [12].
- Stochastic cell biology, a branch of biomathematics seeking to understand how biological systems function in and exploit the presence of noise, uses Brownian motion extensively as a model of noise [13, 14].

In most of the applications listed here, Brownian motion is considered as taking place inside an unbounded region (in $\mathbb{R}$ or $\mathbb{R}^d$). Clearly, it is also important to consider processes undergoing Brownian motion in some bounded region. A simple example of such a process is a diffusion process inside a biological cell, undergoing a chemical reaction at the cell wall [15]. For such processes, both the geometry of the boundary and the behavior of the process at the boundary are important in determining the trajectories of the process. In the case where the process evolves in a bounded region it is therefore necessary that a prescription of the process' behavior upon reaching the boundary be provided in order to complete the description of the system. As an illustration, we show in 1.2 a two-dimensional Brownian motion inside a container with reflecting walls for different geometries of the container. The theory of Brownian motion in a bounded domain is discussed in Schuss [15].

The study of Brownian motion in bounded domains is very active currently, with much of the theory tracing back to Feller, who provided a complete classification of all possible types of boundary behavior in 1 dimension [16, 17, 18]. In particular, this led Feller to discovering a new type of boundary behavior, known as sticky boundary behavior, in which a process spends a finite amount of time at the boundary upon reaching it [18, 19]. While Feller provided a classification of boundaries, and an understanding of these boundaries on the level of the Fokker-Planck equation (and its adjoint) describing a stochastic process, he provided no

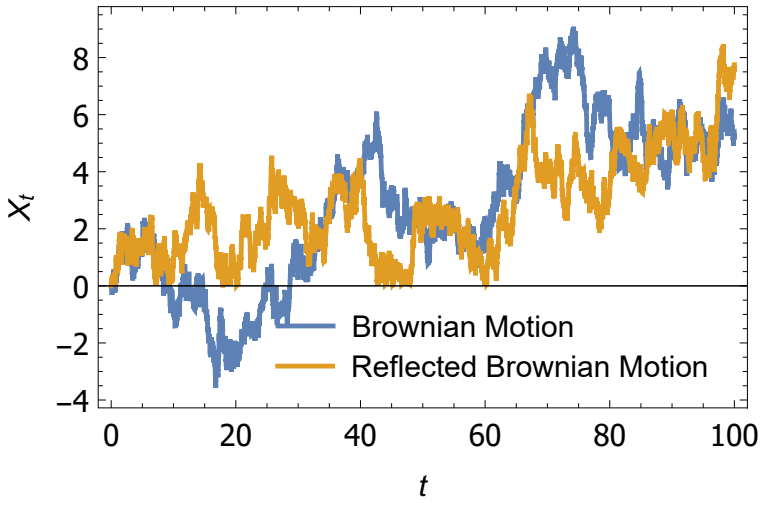

Figure 1.3: Sample paths of Brownian motion and reflected Brownian motion in one dimension.

explicit stochastic construction on the level of a stochastic differential equation of these processes. Skorokhod provided such a construction for reflected diffusions, through the inclusion of so-called local time terms in the stochastic differential equation governing the process [20, 21]. In this thesis we will be particularly interested in processes with reflecting boundary conditions. A survey of results relating to reflected Brownian motion is given in [22]. For illustration, Brownian motion and reflected Brownian motion reflected at the origin are contrasted in Fig. 1.3.

1.2 Large Deviations

The statistical properties of a process X_t are described by the time-dependent probability density $p(x,t) = p(X_t = x)$. In this thesis our goal will not be to study X_t directly, but rather to study the statistical properties of time-integrated functionals or dynamical observables A_T having the form

$$A_T = \frac{1}{T}\int_0^T f(X_t)\,dt. \tag{1.2}$$

In particular, our goal is to describe the probability density $p(A_T = a)$ associated with such a dynamical observable. Examples of such observables include:

- The fraction $\rho_T(y)$ of time (out of a total time T) that the process spends at y. This observable corresponds to the case where $f(x) = \delta(x-y)$ and is called the empirical density at y.
- The mechanical work performed by a laser tweezer on a Brownian particle suspended in water. This observable corresponds to the case where $f(x) =$

x, if the reference frame is chosen to be the co-moving frame of the particle [10].

The probability density $p(A_T = a)$ associated with an observable gives information about both the typical value of the observable and the likelihood of fluctuations away from this typical value. In practice, calculating this density exactly is difficult, even for simple one-dimensional diffusions. For this reason, we appeal to the theory of large deviations, developed by Varadhan [23], which provides a framework within which the long-time behavior of the density $p(A_T = a)$ can be studied. Following this theory, we will see that the density $p(A_T = a)$ often has the asymptotic form

$$p(A_T = a) \approx e^{-TI(a)} \tag{1.3}$$

in the large T limit. An observable A_T whose distribution satisfies this asymptotic form is said to obey a large deviation principle, with the so-called rate function $I(a)$ characterizing the typical value and fluctuations away from this value for the observable in the long-time limit. Large deviation theory has applications in finance, queueing theory and statistical mechanics [24, 25]. It will be our goal in this thesis to obtain the rate function $I(a)$ for reflected diffusions and thereby, to understand the fluctuations of dynamical observables for these types of processes in the long-time limit.

1.3 Goals

The problem of determining the rate function $I(a)$ associated with an observable of a Markov diffusion reduces, as we will see in the next chapter, to finding the dominant eigenvalue of a linear operator [26]. While this problem has been studied extensively and is well understood for diffusions in unbounded domains, the same cannot be said for diffusions in a bounded domain. Here, we will study this problem for bounded diffusions, focusing on one-dimensional diffusions with reflecting boundaries.

The main goal of the thesis, in this context, is to derive the appropriate boundary conditions for the spectral problem associated with finding the rate function. Furthermore, we also wish to understand how the fluctuations of such processes are created dynamically in time. This information is obtained through the study of an 'effective process' introduced by Chetrite and Touchette [27, 28]. We will show that the presence of a reflecting boundary constrains the behavior of this effective process at the boundary.

To illustrate these results, we will obtain the large deviations of the area functional for two reflected processes:

- The reflected Ornstein-Uhlenbeck process [29, 30], which has applications in finance and neuroscience [31] and in queueing theory, where it arises as an approximating process in the high load limit [30].

- Reflected Brownian motion with drift, which represents the motion of a Brownian particle under the influence of gravity in a container.

For each of the cases above we also obtain the effective process associated with the fluctuations of the area observable. In order to obtain a richer understanding of these effective processes, we seek to model them with an appropriate approximation. This is done by using a variational representation of the rate function which is introduced in [32].

1.4 Previous Works

Large deviations of Markov processes have been studied since the works of Donsker and Varadhan in the 1970s [33]. Since then, many studies have looked at large deviations for compact processes [34] (e.g. on the torus) and unbounded diffusions, with few studies, by comparison, on bounded diffusions with explicit boundary behavior specified (e.g. reflection).

The study closest to the work done in this thesis is that of Fatalov [35], where the large deviations of a specific class of observables (which includes, as a special case, the area observable) is obtained by solving a spectral problem. However, this study makes no reference to the origin of the boundary conditions used in this calculation and, furthermore, does not study the effective process which describes how fluctuations are created in time.

The same applies for a paper of Grebenkov [36], in which large deviations are obtained for observables related to the residence time for reflected diffusions. Forde, in [37], also studies large deviations for the time spent at the boundaries of a doubly-reflected Brownian motion, and derives the necessary boundary conditions needed for this calculation, although the specific techniques used differ substantially from ours.

In a more general way, Pinsky [38, 39] and Budhiraja and Dupuis [40] study the large deviations of bounded diffusions, but does so in terms of the so-called level 2 large deviations, a framework which is not used in this thesis.

Finally, studies of large deviations of bounded diffusions in the low-noise limit include Ignatyuk [41], Sheu [42], Dupuis [43], Bo and Zhang [44] and Sheu [42]. In this thesis we do not study the low-noise limit, instead obtaining large deviations in the large-time limit.

1.5 Outline

The thesis is structured as follows. In Chapter 2 we introduce, in the context of stochastic differential equations, the elements of large deviation theory that will be relevant for the discussions and calculations in this thesis. In Chapter 3 we first discuss some general considerations relating to diffusions with boundaries before turning to the specifics of the mathematical implementation of reflecting boundary conditions in one dimension. Finally we discuss how large deviations

are obtained for this class of diffusions. In Chapter 4 the mathematical tools developed in Chapters 2 and 3 are applied in obtaining the large deviations of a dynamical observable for two examples: the reflected Ornstein-Uhlenbeck process in one dimension and reflected Brownian motion with drift in one dimension. We present our conclusions and discuss open problems and possible extensions of our work in Chapter 5.

Chapter 2

Large Deviations of Markov Diffusions

In this chapter we introduce those aspects of the mathematical theory of stochastic differential equations (SDEs) and the theory of large deviations, as applied to Markov diffusions governed by an SDE, that will be needed for the subsequent calculations and discussions of Chapters 3 and 4. Our introduction to the theory of large deviations is based on [45] and especially [26]. Applications of large deviation theory in statistical mechanics are discussed in [24]. For a comprehensive introduction to large deviation theory, see Dembo and Zeitouni [25]. For an introduction to probability theory and stochastic processes the reader is referred to [46]. A good reference for stochastic methods in physics is Gardiner [8].

2.1 Stochastic Differential Equations

We consider a continuous-time Markov diffusion X_t satisfying a *stochastic differential equation* (SDE) of the form

$$dX_t = F(X_t)\,dt + \epsilon(X_t)\,dW_t, \tag{2.1}$$

where

- $X_t \in \mathbb{R}^d$ is the state of the system at $t \in \mathbb{R}^+$
- $F : \mathbb{R}^d \to \mathbb{R}^d$ is the *force* or *drift* that describes the deterministic part of the evolution of X_t in the absence of any noise ($\epsilon = 0$).
- $W_t \in \mathbb{R}^m$ is a vector of independently distributed Wiener motions, whose increments dW_t are Gaussian distributed with mean 0 and variance dt. In general, W_t can have dimension m different from d. The presence of this term is responsible for stochasticity in the evolution of X_t.
- $\epsilon : \mathbb{R}^d \to \mathbb{R}^d \times \mathbb{R}^m$ is the *noise matrix* controlling the strength and type of noise present in the system, and has dimensions to match that of W_t and X_t.

While it is possible for F and ϵ to depend explicitly on the time t, we do not consider this case. We also consider W_t with dimensions the same as that of X_t. The process X_t is Markovian because at every point in time the evolution of X_t depends only on the current state of X_t via F, to which the noise $\epsilon(X_t)\,dW_t$ is added. The process therefore has no 'memory' of the past.

The SDE (2.1) has the formal solution

$$X_T = X_0 + \int_0^T F(X_t)\,dt + \int_0^T \epsilon(X_t)\,dW_t, \tag{2.2}$$

and so we must associate a meaning to the stochastic integral $\int_0^T \epsilon(X_t)dW_t$. The stochastic integral differs from the Riemann integral in that the value of the stochastic integral will depend on the integration convention used, that is, in the manner in which values of the integrand are chosen in each discretisation interval in the sum. An SDE is therefore only completely defined once we also specify the integration convention used in calculating stochastic integrals [1].

The two most commonly used conventions are:

- Itô: The left-most point in each discretization interval is chosen.
- Stratonovich: The midpoint of each discretization interval is chosen.

While an Itô SDE can be transformed into a Stratonovich SDE with a modified drift (and vice versa) [1] we will not discuss these transformations since we will only consider SDEs with a noise ϵ that is independent of X_t. For this case, the stochastic integral does not depend on the convention used. In other words, we will restrict our attention to the case where X_t satisfies the SDE

$$dX_t = F(X_t)\,dt + \epsilon\,dW_t. \tag{2.3}$$

For an introduction to the theory of stochastic differential equations that is appropriate for physicists, the reader is referred to Jacobs [1].

2.2 The Fokker-Planck Operator

The state X_t described by the SDE (2.3) is a random variable whose density $p(x,t) = p(X_t = x)$ as a function of time is known to satisfy the *Fokker-Planck equation*

$$\partial_t p(x,t) = -\nabla \cdot (F(x)p(x,t)) + \frac{1}{2}\nabla \cdot D\nabla p(x,t) \tag{2.4}$$

with initial probability density $p(x,0)$, where $D = \epsilon\epsilon^T$ [47]. For more information regarding the Fokker-Planck equation the reader is referred to Risken [47]. We can rewrite the Fokker-Planck equation in the form

$$\partial_t p(x,t) = \mathcal{L}^\dagger p(x,t), \tag{2.5}$$

where we have introduced the *Fokker-Planck operator* $\mathcal{L}^\dagger$ given by

$$\mathcal{L}^\dagger = -\nabla \cdot F + \frac{1}{2}\nabla \cdot D\nabla. \tag{2.6}$$

The Fokker-Planck operator is a linear operator acting on an appropriate class of probability densities satisfying the relevant boundary conditions of the problem at hand. It is important to note that the form of $\mathcal{L}^\dagger$ as a differential operator is only one part of its definition; to completely define the operator, we must also specify the domain of functions $\mathcal{D}(\mathcal{L}^\dagger)$ on which it acts.

The linearity of the operator $\mathcal{L}^\dagger$ implies that the probability density $p(x,t)$ satisfies

$$p(x,t) = T(t)\, p(x,0) \tag{2.7}$$

with $T(t) = e^{t\mathcal{L}^\dagger}$. The family of operators $\{T(t) : t \geq 0\}$ form a semi-group since they satisfy the semi-group property $T(t+t') = T(t)\,T(t')$ and $T(0) = I$ is satisfied. The semi-group property is the mathematical statement of the Markov property.

The Fokker-Planck equation can also be recast in the form of a conservative equation

$$\partial_t p(x,t) + \nabla \cdot J_p(x,t) = 0 \tag{2.8}$$

with $J_p(x,t)$ representing the time-dependent *probability current* given by

$$J_p(x,t) = F(x)p(x,t) - \frac{1}{2}D\nabla p(x,t). \tag{2.9}$$

The probability current is a vector field describing the spatial flow of probability in time.

If the process is ergodic, it has a unique stationary distribution $p^*(x)$ satisfying

$$\mathcal{L}^\dagger p^*(x) = 0. \tag{2.10}$$

Ergodic processes have the useful property that long-time averages can be replaced by averages with respect to the stationary density p^*. Mathematically stated, an ergodic process X_t satisfies the relation

$$\lim_{T\to\infty} \frac{1}{T}\int_0^T f(X_t)\, dt = \int_{\mathcal{S}} f(x)\, p^*(x)\, dx \tag{2.11}$$

in probability, where $\mathcal{S}$ is the state space of the process X_t.

An important class of SDEs are the so-called *gradient* SDEs for which the drift satisfies $F = -\nabla U$ for some potential U and the noise matrix σ is proportional to the identity matrix, that is $\sigma = \epsilon\mathbb{I}$ for some $\epsilon > 0$. In this case the SDE governing X_t is given by

$$dX_t = -\nabla U(X_t)\, dt + \epsilon\, dW_t. \tag{2.12}$$

Gradient processes are ergodic if the potential is concave and sufficiently steep and have a stationary density p^* given by

$$p^*(x) = \mathcal{N} \exp\left[-\frac{2U(x)}{\epsilon^2}\right] \tag{2.13}$$

known as a *Gibbs density*, with $\mathcal{N}$ a normalization constant. A density of this form has zero current everywhere, as can be checked from (2.9). A particular case of gradient diffusions which we will focus on are SDEs on $\mathbb{R}$ for which the drift can always be written as the derivative of a potential.

2.3 Markov Generator

Having discussed the time evolution of the density $p(x,t)$ we now turn our attention to the time evolution of expectation values, given by

$$\mathbb{E}\left[f(X_t)\right] = \int_{\mathcal{S}} p(x,t) f(x)\, dx \tag{2.14}$$

where $\mathbb{E}[\cdot]$ denotes the expectation on the state space $\mathcal{S}$ of X_t and f is any 'test' function of X_t. Expectation values can be written in a natural way as an inner product

$$\langle p, f\rangle = \int_{\mathcal{S}} p(x) f(x)\, dx \tag{2.15}$$

with p a density and f a test function of the process. Thus, the expectation value (2.14) now takes the form

$$\mathbb{E}\left[f(X_t)\right] = \langle p, f\rangle, \tag{2.16}$$

where it should be understood that p here refers to the time-dependent density $p(x,t)$ at the relevant time t.

The time evolution of this expectation value is given by

$$\partial_t \mathbb{E}\left[f(X_t)\right] = \int_{\mathcal{S}} \partial_t p(x,t) f(x)\, dx = \int_{\mathcal{S}} \left[\mathcal{L}^\dagger p(x,t)\right] f(x)\, dx = \langle \mathcal{L}^\dagger p, f\rangle. \tag{2.17}$$

Based on this, it is natural to define the *adjoint* of the Fokker-Planck operator $\mathcal{L}^\dagger$ with respect to the inner product (2.15) as that operator $\mathcal{L}$ which satisfies

$$\langle \mathcal{L}^\dagger p, f\rangle = \langle p, \mathcal{L} f\rangle. \tag{2.18}$$

Using this relation, we are able to write the time evolution of the expectation value (2.14) in the form

$$\partial_t \mathbb{E}\left[f(X_t)\right] = \langle p, \mathcal{L} f\rangle = \mathbb{E}\left[(\mathcal{L} f)(X_t)\right]. \tag{2.19}$$

Given the presence of the Lebesgue measure dx in (2.15), we say that $\mathcal{L}$ and $\mathcal{L}^\dagger$ are adjoint with respect to the Lebesgue measure. The operator $\mathcal{L}$ is

simply called the *generator* of the process X_t and governs the time evolution of expectation values, as seen in (2.19).

It remains to find the form of the generator $\mathcal{L}$ as a differential operator. We have for a density p and a test function f that

$$\begin{aligned}\langle \mathcal{L}^\dagger p, f\rangle &= \int_{\mathcal{S}} \left[-\nabla(F(x)p(x)) + \frac{1}{2}\nabla\cdot D\nabla p(x)\right] f(x)\,dx \\ &= \int_{\mathcal{S}} p(x)\left[F(x)\cdot\nabla f(x) + \frac{1}{2}\nabla\cdot D\nabla f(x)\right] dx + \text{boundary term},\end{aligned} \tag{2.20}$$

where we have simply used integration by parts and the boundary term is the one that arises in this procedure. In order for the adjoint $\mathcal{L}$ to exist and to be defined independently of p and f, we must have that the boundary term vanishes and therefore, from (2.20) and the definition (2.18), $\mathcal{L}$ has the form

$$\mathcal{L} = F\cdot\nabla + \frac{1}{2}\nabla\cdot D\nabla. \tag{2.21}$$

We note that with respect to the inner product (2.15) we have that $(F\cdot\nabla)^\dagger = -\nabla\cdot F$ (skew-symmetric) and $(\nabla\cdot D\nabla)^\dagger = \nabla\cdot D\nabla$ (Hermitian), so that $\mathcal{L}$ is in general not Hermitian. Moreover, for ergodic processes, the stationary condition $\mathcal{L}^\dagger p^* = 0$ leads, with (2.17) and (2.18), to

$$\mathcal{L}1 = 0, \tag{2.22}$$

where 1 is the constant function on $\mathcal{S}$.

The requirement that the boundary term arising from the integration by parts which relates $\mathcal{L}^\dagger$ and $\mathcal{L}$ vanish will require us to restrict the domain of functions on which $\mathcal{L}$ is defined and give us the boundary conditions for this operator. We will discuss this in more detail in Chapter 3. For more information regarding the generator and its adjoint, see [48].

2.4 Large Deviation Principle

Our goal in this thesis is to study the fluctuations of additive functionals A_T of the process X_t having the form

$$A_T = \frac{1}{T}\int_0^T f(X_t)\,dt. \tag{2.23}$$

Such an additive functional is also known as a time-integrated functional or, in physics, as a *dynamical observable*.

We note the normalization factor of $1/T$ which ensures, according to the ergodic theorem, that A_T converges in probability to its mean value in the limit $T\to\infty$. Mathematically this means that

$$\lim_{T\to\infty} P\left(A_T \in [a^* - \varepsilon, a^* + \varepsilon]\right) = 1 \tag{2.24}$$

for all $\varepsilon > 0$, where

$$a^* = \lim_{T\to\infty} \mathbb{E}\left[A_T\right] = \int_{\mathcal{S}} p^*(x) f(x)\, dx \tag{2.25}$$

is the stationary expected value of A_T. Equivalently, we can state (2.24) in the form

$$\lim_{T\to\infty} p(A_T = a) = \delta(a - a^*), \tag{2.26}$$

where $p(A_T = a)$ is the probability density of A_T.

In the context of this result, we are interested to study the long-time asymptotics of $p(A_T = a)$ around a^* as $T \to \infty$. Following the theory of large deviations [24, 26, 45], we expect the density $p(A_T = a)$ to have the asymptotic form

$$p(A_T = a) = e^{-TI(a)+o(T)} \tag{2.27}$$

for time T large. If this is the case, we say that the observable A_T satisfies a *large deviation principle* with rate function $I(a)$. The meaning of this asymptotic form is that the dominant contribution to the density $p(A_T = a)$ is a decaying exponential in T, with the rate of this decay controlled by the function $I(a)$. Other contributions to the density are sub-exponential in T and are included in the $o(T)$ term. Equivalently, we say that A_T satisfies a large deviation principle if the limit

$$I(a) = \lim_{T\to\infty} -\frac{1}{T} \ln p(A_T = a) \tag{2.28}$$

exists and has a non-trivial value, by which we mean that the rate function is not 0 or ∞ everywhere.

The rate function $I(a)$ satisfies the inequality $I(a) \geq 0$. For those values a for which $I(a) > 0$ the probability density decays exponentially in T, while concentrating on those values a for which $I(a) = 0$. In the case where there is a unique a^* such that $I(a^*) = 0$, this value a^* corresponds to the mean of A_T and gives rise to a law of large numbers: the probability density $p(A_T = a)$ concentrates ever more sharply on a^* as T increases and becomes a Dirac delta centered on a^* in the limit $T \to \infty$. This corresponds to (2.26). For those cases considered in this thesis the rate function will always possess a unique zero.

The rate function $I(a)$ is useful as it provides information regarding the small fluctuations of A_T close to its typical value a^* and the large fluctuations far away from a^*. Generally, the rate function $I(a)$ is not a parabola and so the fluctuations around the mean are not Gaussian. This means that large deviation theory describes fluctuations outside the applicability of the central limit theorem and so serves as a more general theory of fluctuations.

2.5 Scaled Cumulant Generating Function

We now introduce the *scaled cumulant generating function* (SCGF), which will play a central role in the large deviation calculations throughout the thesis. Given

an additive functional A_T having the form (2.23), we define the SCGF as

$$\lambda(k) = \lim_{T\to\infty} \frac{1}{T} \ln \mathbb{E}\left[e^{TkA_T}\right], \quad k \in \mathbb{R}. \tag{2.29}$$

The central role of this function in large deviation calculations is due to the Gärtner-Ellis theorem, which states that if $\lambda(k)$ exists and is differentiable in k, then the following holds:

- A_T satisfies a large deviation principle.
- The rate function $I(a)$ associated with A_T is given by the Legendre-Fenchel transform of $\lambda(k)$:
$$I(a) = \sup_{k\in\mathbb{R}}\{ka - \lambda(k)\}. \tag{2.30}$$

In other words, if $\lambda(k)$ satisfies the conditions stated in the Gärtner-Ellis theorem, the existence of a large deviation principle is immediately established and, moreover, we have a means by which to calculate the rate function $I(a)$ associated with this large deviation principle and thus to determine the probability density $p(A_T = a)$ up to leading order.

The Legendre-Fenchel transform of a function reduces to the Legendre transform if the function is both differentiable and strictly convex (so that there are no linear parts). In that case, the derivative of the function is monotonically increasing and therefore can be inverted, yielding

$$I(a) = k(a)a - \lambda(k(a)) \tag{2.31}$$

where $k(a)$ is the unique solution of

$$\lambda'(k) = a. \tag{2.32}$$

Note from the definition (2.29) that we have $\lambda(0) = 0$ and $\lambda'(0) = a^*$. These properties of the SCGF will prove useful later.

2.6 Large Deviations of Diffusions and the Spectral Problem

Given a Markov diffusion X_t and an additive functional A_T of the form (2.23), we now turn to the question of how the SCGF $\lambda(k)$ is to be found. The relevant mathematical result here is the Feynman-Kac formula, which can be used to show that $\lambda(k)$, if it exists as a SCGF, is the dominant eigenvalue of the linear differential operator $\mathcal{L}_k$, given as

$$\mathcal{L}_k = \mathcal{L} + kf, \tag{2.33}$$

with $\mathcal{L}$ the generator of the process X_t and f the function appearing as the integrand in (2.23). The operator $\mathcal{L}_k$ is known as the *tilted generator*. For the

adjoint operator $\mathcal{L}_k^\dagger$ we have from the definition of the inner product (2.15) and the definition of the adjoint (2.18) that

$$\mathcal{L}_k^\dagger = \mathcal{L}^\dagger + kf \tag{2.34}$$

with $\mathcal{L}^\dagger$ the Fokker-Planck operator of X_t. Notice that kf is a scalar term that is Hermitian. For more information on the link between the Feynman-Kac formula and the SCGF, see [26].

Since $\mathcal{L}$ is not, in general, Hermitian, neither is $\mathcal{L}_k$. This complicates the calculation involved in obtaining the spectrum and therefore the dominant eigenvalue $\lambda(k)$, since we now have to consider not only the direct or 'right' eigenvalue problem

$$\mathcal{L}_k r_k = \lambda(k) r_k \tag{2.35}$$

but also the dual or 'left' eigenvalue problem

$$\mathcal{L}_k^\dagger l_k = \lambda(k) l_k. \tag{2.36}$$

These eigenvalue problems have to be considered in conjunction because the boundary conditions that characterize the spectral problem involve simultaneously the right and left eigenfunctions. The issue of boundary conditions will be discussed in more depth in Chapter 3. For now, we note that the normalization condition

$$\int_{\mathcal{S}} r_k(x) l_k(x)\, dx = 1 \tag{2.37}$$

is applied, with $\mathcal{S} \subset \mathbb{R}^d$ denoting the state space for the process X_t. In addition, since $\mathcal{L}_k^\dagger$ is related to the Fokker-Planck operator which acts on some appropriate space of probability densities, we have the normalization or integrability condition

$$\int_{\mathcal{S}} l_k\, dx = 1 \tag{2.38}$$

for the eigenfunctions of $\mathcal{L}_k^\dagger$. We note that, for $k = 0$, we have $\mathcal{L}_{k=0}^\dagger = \mathcal{L}^\dagger$, so that $l_{k=0} = p^*$, while for $\mathcal{L}_{k=0} = \mathcal{L}$, we have $r_{k=0} = 1$ in agreement with (2.22) so that

$$\int_{\mathcal{S}} r_{k=0}(x)\, l_{k=0}(x)\, dx = \int_{\mathcal{S}} p^*(x)\, dx = 1. \tag{2.39}$$

2.7 Symmetrization Method

We have seen that the spectral problem associated with finding the SCGF is complicated by the fact that the tilted generator $\mathcal{L}_k$ is, in general, not Hermitian. A significant simplification is, however, possible in the case where $\mathcal{L}_k$ has a real spectrum. In this case, we can unitarily transform $\mathcal{L}_k$ to a Hermitian operator $\mathcal{H}_k$ which has the same spectrum as $\mathcal{L}_k$, owing to the fact that unitary transformations preserve the spectrum of an operator. We can then find the SCGF as the dominant eigenvalue of the Hermitian operator $\mathcal{H}_k$ for which the

'right' and 'left' eigenvalue problems are identical, meaning that we only have one class of eigenfunctions to consider instead of two, so that standard methods from quantum mechanics can be applied.

For the case where the SDE under consideration is gradient and ergodic, the spectrum of $\mathcal{L}_k$ is indeed real and the unitary transformation that 'symmetrizes' $\mathcal{L}_k$ to a Hermitian operator $\mathcal{H}_k$ is given explicitly by

$$\mathcal{L}_k \to (p^*)^{1/2}\mathcal{L}_k\,(p^*)^{-1/2} = \mathcal{H}_k \tag{2.40}$$

where p^* is the Gibbs stationary density associated with the process X_t given by (2.13). The operator $\mathcal{H}_k$ acts on a function ϕ in the manner

$$\mathcal{H}_k\phi = (p^*)^{1/2}\left(\mathcal{L}_k\left((p^*)^{-1/2}\phi\right)\right). \tag{2.41}$$

From this it can be verified that the explicit form of the operator $\mathcal{H}_k$ is

$$\mathcal{H}_k = \frac{\epsilon^2}{2}\nabla^2 - \mathcal{V}_k \tag{2.42}$$

where $\mathcal{V}_k$ is the quantum-like potential

$$\mathcal{V}_k(x) = \frac{|\nabla U(x)|^2}{2\epsilon^2} - \frac{\nabla^2 U(x)}{2} - kf(x), \tag{2.43}$$

with U the potential for the SDE under consideration. The spectral problem thus becomes

$$\mathcal{H}_k\psi_k = \lambda(k)\psi_k \tag{2.44}$$

with the eigenfunction ψ_k related to r_k and l_k by

$$\psi_k(x) = p^*(x)^{1/2}\,r_k(x) \quad \text{and} \quad \psi_k(x) = p^*(x)^{-1/2}\,l_k(x) \tag{2.45}$$

with the normalization condition (2.37) reducing to

$$\int_{\mathcal{S}} \psi_k(x)^2\,dx = 1. \tag{2.46}$$

We can therefore regard $\mathcal{H}_k$ as a quantum-like Hermitian operator acting on the space of square-integrable functions satisfying the appropriate boundary conditions for the problem at hand. This is exactly the situation encountered in solving the spectral problem for the Schrödinger operator.

2.7.1 Example: Ornstein-Uhlenbeck Process with Linear Observable

As an illustration of the ideas developed up to this point, we consider the *Ornstein-Uhlenbeck process* in one dimension, satisfying the SDE

$$dX_t = -\gamma X_t\,dt + \epsilon\,dW_t, \tag{2.47}$$

with X_t taking values in $\mathbb{R}$ and $\gamma, \epsilon > 0$, where γ is regarded as a friction constant. We are interested in the large deviations of the additive functional A_T given by

$$A_T = \frac{1}{T}\int_0^T X_t\, dt. \tag{2.48}$$

The SDE (2.47) is gradient with the associated potential given by $U(x) = \gamma x^2/2$, such that $F(x) = -\gamma x = -\frac{d}{dx}U(x)$, and with the normalized Gibbs density given by

$$p^*(x) = \sqrt{\frac{\gamma}{\pi\epsilon^2}}\exp\left[-\frac{\gamma x^2}{\epsilon^2}\right]. \tag{2.49}$$

For the SDE (2.47), the generator $\mathcal{L}$ is given from (2.21) by

$$\mathcal{L} = -\gamma x\frac{d}{dx} + \frac{\epsilon^2}{2}\frac{d^2}{dx^2} \tag{2.50}$$

so that the tilted generator associated with this process and observable is given as

$$\mathcal{L}_k = -\gamma x\frac{d}{dx} + \frac{\epsilon^2}{2}\frac{d^2}{dx^2} + kx. \tag{2.51}$$

This operator is not Hermitian and thus obtaining its spectrum directly will prove to be difficult. The SDE under consideration is gradient and so $\mathcal{L}_k$ has a real spectrum and symmetrization is possible. The symmetrized operator $\mathcal{H}_k$ can be found from (2.42) by substituting $U(x) = \gamma x^2/2$ into the expression (2.43) to obtain

$$\mathcal{H}_k = \frac{\epsilon^2}{2}\frac{d^2}{dx^2} - \frac{\gamma^2 x^2}{2\epsilon^2} + \frac{\gamma}{2} + kx. \tag{2.52}$$

The SCGF $\lambda(k)$ is therefore found as the dominant eigenvalue of the spectral problem

$$\left[\frac{\epsilon^2}{2}\frac{d^2}{dx^2} - \frac{\gamma^2 x^2}{2\epsilon^2} + \frac{\gamma}{2} + kx\right]\psi_k^{(n)}(x) = \lambda_n(k)\,\psi_k^{(n)}(x) \tag{2.53}$$

with the eigenfunctions $\psi_k^{(n)}(x)$ satisfying the natural quantum boundary conditions

$$\lim_{|x|\to\infty}\psi_k^{(n)}(x)^2 = 0. \tag{2.54}$$

This boundary condition for the eigenfunctions $\psi_k^{(n)}$ follow from the normalization condition (2.46) which requires that the square of $\psi_k^{(n)}$ decays sufficiently fast to 0 as $|x| \to \infty$.

Introducing the variable $z = x - \epsilon^2 k/\gamma^2$, we find that (2.53) can be written in terms of z as

$$\left[\frac{-\epsilon^2}{2}\frac{d^2}{dz^2} + \frac{\gamma^2 z^2}{2\epsilon^2}\right]\phi_k^{(n)}(z) = \left[\frac{\epsilon^2 k^2}{2\gamma^2} + \frac{\gamma}{2} - \lambda_n(k)\right]\phi_k^{(n)}(z) \tag{2.55}$$

where we have multiplied throughout by -1 and introduced

$$\phi_k^{(n)}(z) = \psi_k^{(n)}\left(z + \frac{k\epsilon^2}{\gamma^2}\right). \tag{2.56}$$

Upon identifying $\gamma = \hbar\omega$ and $\epsilon = \hbar/\sqrt{m}$, we observe that (2.55) is simply the time-independent Schrödinger equation for the quantum harmonic oscillator. We therefore have that the spectrum $\lambda_n(k)$ of the operator $\mathcal{H}_k$ satisfies

$$\frac{\epsilon^2 k^2}{2\gamma^2} + \frac{\gamma}{2} - \lambda_n(k) = \gamma\left(n + \frac{1}{2}\right), \quad n = 0, 1, 2, \ldots \tag{2.57}$$

so that $\lambda_n(k) = \epsilon^2 k^2/2\gamma^2 - \gamma n$, with the dominant eigenvalue and SCGF consequently given by

$$\lambda(k) = \frac{\epsilon^2 k^2}{2\gamma^2}. \tag{2.58}$$

The dominant eigenfunction ϕ_k corresponds to the ground state eigenfunction of the quantum harmonic oscillator and is given by

$$\phi_k(z) = \left(\frac{\gamma}{\pi\epsilon^2}\right)^{1/4} \exp\left[-\frac{\gamma z^2}{2\epsilon^2}\right] \tag{2.59}$$

so that the dominant eigenfunction ψ_k of $\mathcal{H}_k$ is found from (2.56) as

$$\psi_k(x) = \phi_k\left(x - \frac{k\epsilon^2}{\gamma^2}\right) = \left(\frac{\gamma}{\pi\epsilon^2}\right)^{1/4} \exp\left[\frac{-\gamma\left(x - \epsilon^2 k/\gamma^2\right)^2}{2\epsilon^2}\right]. \tag{2.60}$$

The SCGF $\lambda(k)$ is clearly differentiable in k and thus satisfies the conditions of the Gärtner-Ellis theorem. We can therefore find the rate function $I(a)$ associated with A_T as the Legendre-Fenchel transform of $\lambda(k)$. Given that $\lambda(k)$ is strictly convex in k, the Legendre-Fenchel transform reduces to a Legendre transform with $I(a)$ given from (2.31) by

$$I(a) = \frac{\gamma^2 a^2}{2\epsilon^2}. \tag{2.61}$$

The rate function $I(a)$, shown in Fig. 2.1, possesses a single zero at $a^* = 0$ which represents the mean and typical value of A_T. Given the parabolic form of $I(a)$ the system possesses Gaussian fluctuations for values of a around $a^* = 0$.

We can find the right and left eigenfunctions r_k and l_k associated with the dominant eigenvalue $\lambda(k)$ by substituting (2.60) and (2.49) into the relations (2.45) and apply the normalization conditions (2.37) and (2.38) to obtain

$$r_k(x) = \exp\left[\frac{kx}{\gamma} - \frac{3\epsilon^2 k^2}{4\gamma^3}\right] \tag{2.62}$$

and

$$l_k(x) = \sqrt{\frac{\gamma}{\pi\epsilon^2}} \exp\left[-\frac{\gamma(x - \epsilon^2 k/2\gamma^2)^2}{\epsilon^2}\right]. \tag{2.63}$$

We note that, while the product $r_k(x)l_k(x)$ is normalized, the eigenfunction $r_k(x)$ by itself is not normalizeable and blows up as $x \to \infty$ for $k > 0$ and as $x \to -\infty$ for $k < 0$.

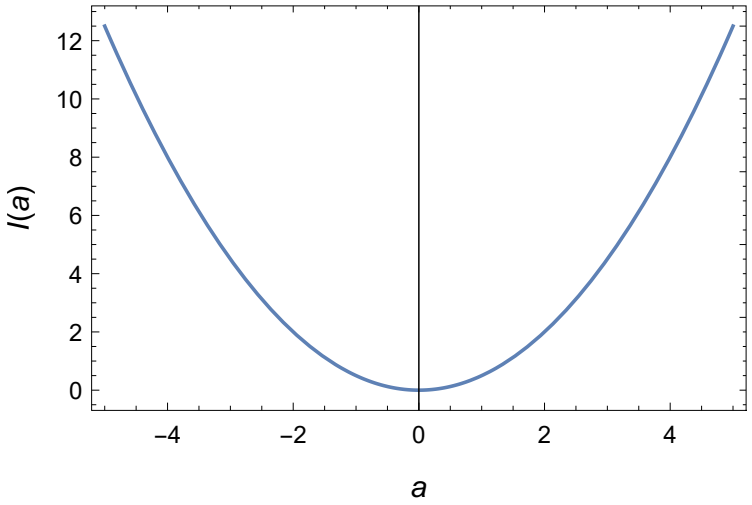

Figure 2.1: Rate function $I(a)$ for the linear observable of the Ornstein-Uhlenbeck process with parameters $\epsilon = 1$ and $\gamma = 1$.

2.7.2 Example: Ornstein-Uhlenbeck Process with Quadratic Observable

As another example, we consider once again the Ornstein-Uhlenbeck process, where we are now interested in the additive functional V_T given by

$$V_T = \frac{1}{T}\int_0^T X_t^2\, dt. \tag{2.64}$$

The stationary distribution and generator of the process X_t remain the same as before, given respectively by (2.49) and (2.50). For the functional V_T the tilted generator $\mathcal{L}_k$ is given by

$$\mathcal{L}_k = -\gamma x\frac{d}{dx} + \frac{\epsilon^2}{2}\frac{d^2}{dx^2} + kx^2. \tag{2.65}$$

The tilted generator is still not Hermitian and therefore we will solve the spectral problem associated with the symmetrized operator $\mathcal{H}_k$, which has the form

$$\mathcal{H}_k = \frac{\epsilon^2}{2}\frac{d^2}{dx^2} - \frac{\gamma^2 x^2}{2\epsilon^2} + \frac{\gamma}{2} + kx^2. \tag{2.66}$$

The SCGF $\lambda(k)$ associated with V_T is therefore determined by solving the spectral problem

$$\left[\frac{\epsilon^2}{2}\frac{d^2}{dx^2} - \frac{\gamma^2 x^2}{2\epsilon^2} + \frac{\gamma}{2} + kx^2\right]\psi_k^{(n)}(x) = \lambda_n(k)\,\psi_k^{(n)}(x), \tag{2.67}$$

where the eigenfunctions $\psi_k^{(n)}$ again satisfy the natural quantum boundary condition

$$\lim_{|x|\to\infty}\psi_k^{(n)}(x)^2 = 0 \tag{2.68}$$

due to the normalization condition (2.46). Multiplying (2.67) throughout by -1 and rearranging terms we arrive at

$$\left[\frac{-\epsilon^2}{2}\frac{d^2}{dx^2} + \frac{x^2(\gamma^2 - 2\epsilon^2 k)}{2\epsilon^2}\right]\psi_k^{(n)}(x) = \left[\frac{\gamma}{2} - \lambda_n(k)\right]\psi_k^{(n)}(x). \tag{2.69}$$

For $k \leq \gamma^2/2\epsilon^2$, the potential is confining and corresponds to the Schrödinger equation for the quantum harmonic oscillator with $\epsilon = \hbar/\sqrt{m}$ and $\sqrt{\gamma^2 - 2\epsilon^2 k} = \hbar\omega$. For $k > \gamma^2/2\epsilon^2$, on the other hand, the potential is not confining and no eigenfunctions exist. We therefore have that for $k \leq \gamma^2/2\epsilon^2$, the spectrum $\lambda_n(k)$ satisfies

$$\lambda_n(k) - \frac{\gamma}{2} = -\sqrt{\gamma^2 - 2\epsilon^2 k}\left(n + \frac{1}{2}\right), \quad n = 0, 1, 2, \ldots \tag{2.70}$$

so that the dominant eigenvalue $\lambda(k)$ is

$$\lambda(k) = \frac{\gamma}{2} - \frac{1}{2}\sqrt{\gamma^2 - 2\epsilon^2 k}, \quad k \leq \frac{\gamma^2}{2\epsilon^2}. \tag{2.71}$$

The SCGF satisfies the conditions of the Gärtner-Ellis theorem, so that the rate function $I(v)$ is found as the Legendre transform of $\lambda(k)$. We find for $I(v)$ that

$$I(v) = \frac{\gamma^2 v}{2\epsilon^2} + \frac{\epsilon^2}{8v} - \frac{\gamma}{2} \tag{2.72}$$

for $v > 0$ since $V_T \geq 0$ by definition and $I(v)$ is not defined for $v = 0$. The rate function $I(v)$ is shown in Fig. 2.2. We note that the zero v^* of the rate function, and therefore the mean of the functional V_T, can be found from (2.72) to be $v^* = \epsilon^2/(2\gamma)$. For the parameters used in Fig 2.2 this becomes $v^* = 1/2$.

The normalized dominant eigenfunction ψ_k associated with the dominant eigenvalue $\lambda(k)$ is given by

$$\psi_k(x) = \left(\frac{\sqrt{\gamma^2 - 2\epsilon^2 k}}{\pi\epsilon^2}\right)^{1/4} \exp\left[-\frac{x^2}{2\epsilon^2}\sqrt{\gamma^2 - 2\epsilon^2 k}\right], \tag{2.73}$$

with r_k and l_k found, as before, by substituting our expressions for ψ_k and p^* into the relations (2.45), yielding

$$r_k(x) = \left(\frac{2\sqrt{\gamma^2 - 2\epsilon^2 k}}{\sqrt{\gamma^2 - 2\epsilon^2 k} + \gamma}\right)^{1/2} \exp\left[-\frac{x^2}{2\epsilon^2}\left(\sqrt{\gamma^2 - 2\epsilon^2 k} - \gamma\right)\right] \tag{2.74}$$

and

$$l_k(x) = \left(\frac{\sqrt{\gamma^2 - 2\epsilon^2 k} + \gamma}{2\pi\epsilon^2}\right)^{1/2} \exp\left[-\frac{x^2}{2\epsilon^2}\left(\sqrt{\gamma^2 - 2\epsilon^2 k} + \gamma\right)\right], \tag{2.75}$$

where we have applied the normalization conditions (2.37) and (2.38).

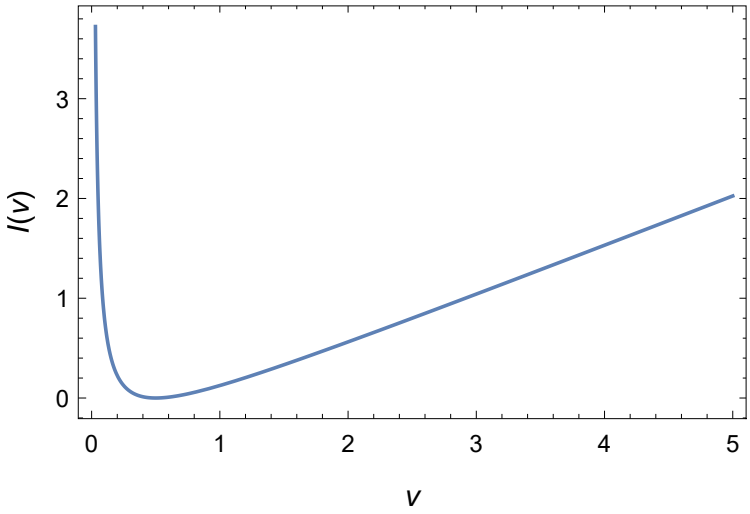

Figure 2.2: Rate function $I(v)$ for the quadratic observable of the Ornstein-Uhlenbeck process with parameters $\epsilon = 1$ and $\gamma = 1$.

2.8 Driven Process

Up to this point we have discussed how to obtain the large deviation functions (the SCGF and the rate function) associated with a time-integrated observable A_T of a Markov diffusion X_t. While these functions are of central importance in understanding the fluctuations of A_T, they provide no information as to how these fluctuations are created dynamically in time.

Recently, Chetrite and Touchette [27, 28] have shown that this information is provided by a modified Markov process, called the *effective* or *driven process*, which essentially corresponds to the long-time limit of the process X_t conditioned on obtaining a given fluctuation $A_T = a$ and which thus realizes trajectories giving rise to the fluctuation $A_T = a$.

In the case where the rate function $I(a)$ is convex the effective process is labelled by the parameter k of the SCGF $\lambda(k)$. It is shown in [27] that for a process having an SDE of the form (2.3), the driven process $X_t^{(k)}$ realizing the fluctuation $A = a(k) = \lambda'(k)$ satisfies the SDE

$$dX_t^{(k)} = F_k(X_t)\,dt + \epsilon\,dW_t \tag{2.76}$$

with the *driven force* F_k given in terms of the eigenfunction r_k, corresponding to the dominant eigenvalue $\lambda(k)$ of the tilted generator, as

$$F_k(x) = F(x) + D\nabla \ln r_k(x). \tag{2.77}$$

The driven process can be regarded as a process which has the atypical trajectories of X_t for which $A_T = a$ as typical trajectories. We therefore have for the driven process that

$$\lim_{T\to\infty} \frac{1}{T} \int_0^\infty f\left(X_t^{(k)}\right) dt = a(k) \tag{2.78}$$

in probability.

For a gradient process X_t having an SDE (2.12) and a Gibbs density (2.13), symmetrization is possible and the driven force can be written with (2.45) in terms of the eigenfunction ψ_k associated with the Hermitian operator $\mathcal{H}_k$. We have from (2.45) that

$$F_k(x) = F + D\nabla \ln \left(p^*(x)^{-1/2}\psi_k(x)\right) \tag{2.79}$$

which becomes, noting that $D = \epsilon^2 \mathbb{I}$,

$$F_k(x) = F - \frac{\epsilon^2}{2}\nabla \ln p^*(x) + \epsilon^2 \nabla \ln \psi_k. \tag{2.80}$$

From the definition of the Gibbs density (2.13), and the fact that $F = -\nabla U$, this reduces to

$$F_k(x) = \epsilon^2 \nabla \ln \psi_k = \epsilon^2 \frac{\nabla \psi_k(x)}{\psi_k(x)}. \tag{2.81}$$

Equivalently we can describe the driven process in terms of an *effective* or *driven potential* U_k associated with the force F_k and satisfying $\nabla U_k = -F_k$ as

$$U_k(x) = -\epsilon^2 \ln \psi_k(x). \tag{2.82}$$

We note that this last relation implies that we can write

$$\psi_k(x)^2 = r_k(x) l_k(x) = \mathcal{N} \exp\left[-\frac{2U_k(x)}{\epsilon^2}\right], \tag{2.83}$$

with $\mathcal{N}$ being a normalization constant, and so we can interpret the product ψ_k^2 or $r_k l_k$ as being the stationary Gibbs density associated with the drift F_k. That is, ψ_k^2 is the stationary density of the effective process that realizes the fluctuation associated with the parameter k. We will denote this stationary density with potential U_k as p_k in the following, so that

$$p_k(x) = \psi_k(x)^2 = r_k(x) l_k(x). \tag{2.84}$$

2.8.1 Example: Ornstein-Uhlenbeck Process with Linear Observable

To illustrate the notion of the driven process, we return now to the Ornstein-Uhlenbeck process on the real line that was studied in Section 2.5.1. We are interested in obtaining the driven process associated with the linear functional A_T studied there. This process is gradient and so we can obtain the driven force F_k from the relation (2.81). Substituting the expression (2.60) for the eigenfunction ψ_k into (2.81) yields

$$F_k(x) = -\gamma\left(x - \frac{\epsilon^2 k}{\gamma^2}\right), \tag{2.85}$$

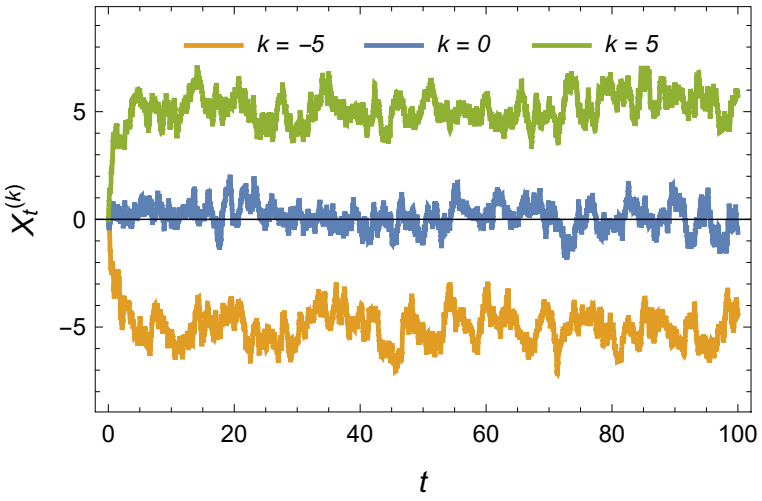

Figure 2.3: Sample paths for the normal Ornstein-Uhlenbeck process X_t ($k = 0$) and the driven processes $X_t^{(k)}$ for $k = -5$ and $k = 5$ are shown for the parameters $\epsilon = 1$ and $\gamma = 1$.

while the effective potential U_k found by substituting (2.60) into (2.82) is

$$U_k(x) = \gamma \left(x - \frac{\epsilon^2 k}{\gamma^2} \right)^2 . \tag{2.86}$$

The driven process $X_t^{(k)}$ associated with the fluctuation $A_T = a(k)$ is therefore given by

$$dX_t^{(k)} = -\gamma \left(x - \frac{\epsilon^2 k}{\gamma^2} \right) dt + \epsilon \, dW_t, \tag{2.87}$$

where we note that $a(k) = \lambda'(k) = \epsilon^2 k/\gamma^2$ from (2.58). These expressions can all be parameterized by the fluctuation value $A_T = a$ instead of k simply by using the relation $a = \lambda'(k) = \epsilon^2 k/\gamma^2$.

Sample paths of the process $X_t^{(k)}$ are shown in Fig. 2.3. We observe that the trajectory of the process $X_t^{(k)}$ spends the majority of the time close to the value $a(k) = \epsilon^2 k/\gamma^2$. This can be understood from the expression of F_k which has a zero at $x = a(k) = \epsilon^2 k/\gamma^2$ and therefore shifts the stable equilibrium of the process from $x = 0$ to $a(k)$, implying in the long-time limit that $A_T \to a(k)$ or, equivalently, $A_T \to a$ if we parameterize $X_t^{(k)}$ in terms of a instead of k. The zero of F_k corresponds in the potential U_k to a position of minimum 'energy' for the system, with the potential U_k having a minimum at $a(k) = \epsilon^2 k/\gamma^2$.

2.8.2 Example: Orsntein-Uhlenbeck process with Quadratic Functional

We now obtain the driven process associated with the quadratic functional V_t of the Ornstein-Uhlenbeck process. Following the procedure just used, the driven

force F_k is obtained by substituting the eigenfunction (2.73) into (2.81), yielding

$$F_k(x) = -x\sqrt{\gamma^2 - 2\epsilon^2 k}, \quad k \leq \frac{\gamma^2}{2\epsilon^2}. \tag{2.88}$$

The driven potential U_k associated with the force F_k is thus found from (2.82) to be

$$U_k(x) = \frac{x^2}{2}\sqrt{\gamma^2 - 2\epsilon^2 k}, \quad k \leq \frac{\gamma^2}{2\epsilon^2}. \tag{2.89}$$

Both F_k and U_k are associated with the fluctuation $v(k)$ depending on k in the manner

$$v(k) = \lambda'(k) = \epsilon^2/2\sqrt{\gamma^2 - 2\epsilon^2 k}, \quad k \leq \frac{\gamma^2}{2\epsilon^2} \tag{2.90}$$

where we have used the expression (2.71) for the SCGF $\lambda(k)$. The driven process $X_t^{(k)}$ which realizes a fluctuation $v(k) = \epsilon^2/2\sqrt{\gamma^2 - 2\epsilon^2 k}$ as a typical value therefore satisfies the SDE

$$dX_t^{(k)} = -X_t^{(k)}\sqrt{\gamma^2 - 2\epsilon^2 k}\, dt + \epsilon\, dW_t \quad \text{for} \quad k \leq \frac{\gamma^2}{2\epsilon^2}. \tag{2.91}$$

As before, we can also parameterize $X_t^{(k)}$ in terms of v using the relation $v(k) = v$.

We note that while the driven force (2.85) for the linear functional A_T involved a constant shift and that this manifested itself in the trajectories of $X_t^{(k)}$ as being shifted to spending the majority of the time T close to the fluctuation a_k, the driven force for the functional V_T scales the friction of $X_t^{(k)}$ by a factor depending on k.

Sample paths of the driven process (2.91) are shown in Fig. 2.4. We observe for $k < 0$ that the size of the excursions away from $x = 0$ are, on average, smaller than those for $k = 0$, because of the larger friction, thus forcing $X_t^{(k)}$ to realize smaller values of V_T. For $k > 0$, on the other hand, the average excursions away from $x = 0$ are larger than for $k = 0$, because of a smaller friction, leading to larger values of V_T. In the limit where $k \to \gamma^2/(2\epsilon^2)$, $F_k \to 0$ so that the very large fluctuations of V_T are effectively realized by Brownian motion which undergoes arbitrarily large excursions away from $x = 0$.

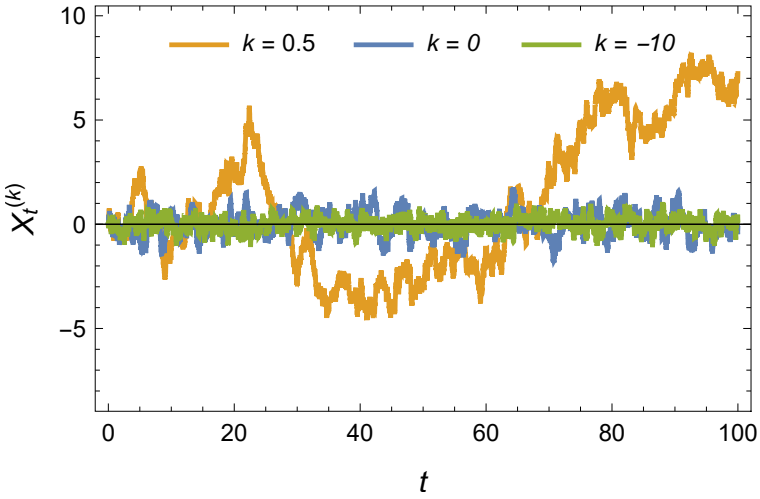

Figure 2.4: Sample paths for the normal Ornstein-Uhlenbeck process X_t $(k = 0)$ and the driven processes $X_t^{(k)}$ for $k = 0.5$ and $k = -10$ are shown for the parameters $\epsilon = 1$ and $\gamma = 1$.

Chapter 3

Large Deviations of Reflected Diffusions

In this chapter we study the physical and mathematical role played by boundary conditions on the behavior of Markov diffusions. We discuss various types of boundaries commonly used in practice and discuss a classification of such boundaries, focusing on one dimensional diffusions. With this background we then turn our attention to the large deviations of time-integrated functionals of reflected diffusions and determine the manner in which reflecting boundary conditions influence the spectral problem associated with obtaining the SCGF.

3.1 Diffusions with Boundaries

We consider a d-dimensional Markov diffusion X_t evolving in some region $\mathcal{E} \subset \mathbb{R}^d$ with a boundary $\partial\mathcal{E}$ assumed to be a smooth $(d-1)$-dimensional surface in $\mathbb{R}^d$. While the behavior of the process in the interior of $\mathcal{E}$ is determined by its SDE, a separate prescription is needed for the behavior of the process at the boundary $\partial\mathcal{E}$ in the event that this boundary is reached.

Many such prescriptions are used in practice. Following what we have discussed in Chapter 1, we list some commonly used prescriptions:

- **Absorbing boundaries**: The process X_t is terminated upon reaching the boundary or, equivalently, remains indefinitely on the boundary upon reaching it. Consider as an example a process $X_t \in [0, \infty)$ representing the concentration of a biological population occupying some region. In the event where immigration into this region is not possible, a population that reaches 0 will remain at 0 indefinitely. The boundary $\{0\}$ is therefore considered an absorbing boundary for this process.

- **Reflecting boundaries**: Upon reaching such a boundary, the process is reflected instantaneously in a specular manner similar to light reflecting off a mirror or the elastic reflection of a particle upon striking a wall. A

particle undergoing Brownian motion inside a container with hard walls is an example of a process with reflecting boundaries.

- **Elastic or partially reflecting boundaries**: A boundary is said to be elastic or partially reflecting if the process is reflected with some probability p and absorbed with probability $1 - p$ upon reaching this boundary. Partially reflecting boundaries are encountered in biology and chemistry in the study of processes with reactive boundaries [15].

- **Sticky boundaries**: A boundary is sticky if a process, upon reaching it, is required to remain there for some fixed or random amount of time before being allowed to re-enter the interior of the state space [19, 18].

- **Instantaneous return process**: For such a process we have that, upon reaching the boundary, X_t is placed in the interior of $\mathcal{E}$ according to some probability distribution. The process then continues to evolve according to the SDE which governs its evolution.

Discussions of the types of boundaries listed here can be found in [15] and [49].

At this point it must be noted that the question of whether a boundary can be reached (with non-zero probability) or not is of importance. Clearly the behavior of the process X_t need only be defined at a boundary if that boundary can be reached from the interior $\mathcal{E}^\circ$ of $\mathcal{E}$. In probability theory, a boundary is called *accessible* if, starting from an initial point inside the interior $\mathcal{E}^\circ$, the process reaches the boundary in finite expected time. If this is not the case, the boundary is called *inaccessible* [49]. Accessible boundaries are further subdivided as

- **Regular**: A boundary is regular if the boundary can be attained from the interior $\mathcal{E}^\circ$ and also if the process can re-enter the interior $\mathcal{E}^\circ$ from the boundary.

- **Exit**: An exit boundary can be reached from $\mathcal{E}^\circ$, but once the process has reached this boundary it can never re-enter the interior (e.g. if the boundary is absorbing).

On the other hand, inaccessible boundaries are classified as

- **Entrance**: A process can reach the interior from such a boundary, although the boundary itself can never be reached from the interior. In other words a process can start on such a boundary but once entering the interior $\mathcal{E}^\circ$ will never reach this boundary again.

- **Natural**: A process can neither be started at such a boundary nor reach it from the interior in finite time. This boundary can be regarded as outside the state space of the process X_t. We have encountered natural boundaries before, for example at $-\infty$ and ∞ in our consideration of the Ornstein-Uhlenbeck process on $\mathbb{R}$.

This classification of boundaries was proposed by Feller [16] and is known as the Feller classification. In one dimension, conditions on the drift F and noise ϵ for a boundary being of a given type are well-known and discussed in, for example, [49].

In this thesis we consider diffusions in one dimension with reflecting boundaries that are accessible and regular. This type of boundary behavior was first studied on the level of the SDE for Brownian motion in 1961 by Skorokhod [20, 21], who showed that this type of boundary can be implemented mathematically through the addition of a new term, corresponding to the so-called local time, in an SDE.

This result, now known as the Skorokhod construction, is too technical for our needs and will not be considered here. Instead, we take a more practical approach in which we solve the SDE in the interior of $\mathcal{E}$ in the usual manner and reflect mechanically the system's state if it attempts to cross the boundary, as is done in ordinary differential equations. As will be shown, this procedure implies a boundary condition for the Fokker-Planck equation, which is usually how reflections are treated mathematically in physics. This manner of implementing the boundary condition is mathematically simpler and intuitively more appealing, given the physical nature of the Fokker-Planck operator as the generator of time evolution of the probability density describing the system's state.

In this thesis we will restrict ourselves to one dimensional diffusions. The treatment of boundaries in dimensions higher than one is mathematically much more complex and it is, in fact, still a research problem to understand the effect of complicated boundaries in two or three dimensions [15].

3.2 Reflected Diffusions in One Dimension

We consider from now on the case where X_t is a Markov diffusion in one dimension satisfying an SDE of the form

$$dX_t = F(X_t)\,dt + \epsilon\,dW_t, \tag{3.1}$$

on the interval $[a, b]$, with $a < b$ and with reflecting boundary conditions at $x = a$ and $x = b$. The reflection is implemented in simulations as in ordinary differential equations by reflecting the state when it "crosses" the boundary. To be more precise, consider the evolution of X_t, representing the position of a Brownian particle, over a small time interval Δt as determined [50, 15] by the Euler-Maruyama (or simply Euler) scheme

$$X_{t+\Delta t} = X_t + F(X_t)\,\Delta t + \epsilon\,\Delta W_t, \tag{3.2}$$

where ΔW_t is a Gaussian random variable with mean 0 and variance Δt. The particle can move closer to the boundary without crossing it if it is initially far enough from it, as shown in Fig. 3.1a. However, as it gets close enough to the boundary, it is possible that the state X_t updated to $X_{t+\Delta t}$ can cross the

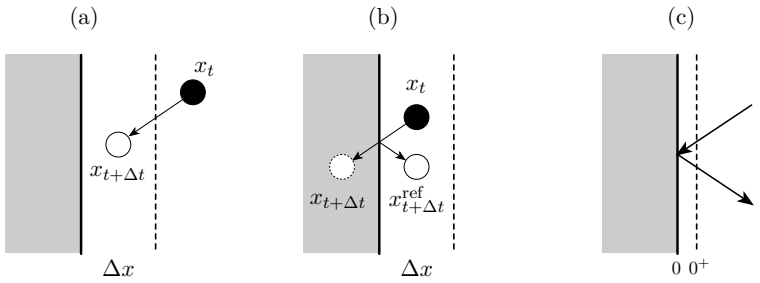

Figure 3.1: (a): Illustration of zero current conditions at a reflecting boundary. (b): Discretization of a reflection at a boundary where $x^{\text{ref}}_{t+\Delta t}$ is the final position of the particle after reflection has been applied. (c) Boundary layer introduced by the discretization becoming infinitesimal as $\Delta t \to 0$.

boundary, as shown in Fig. 3.1b. In this case, the state $X_{t+\Delta t}$ is reflected to $-X_{t+\Delta t}$ to account for the reflection.

The typical distance Δx from the boundary within which X_t can cross the boundary within a single time step is known as the *boundary layer*. In general, the thickness of this layer, which represents an error or artefact of the Euler-Maruyama scheme, decreases to 0 as $\Delta t \to 0$, with Fig. 3.1c representing this limit, where the boundary layer now has infinitesimal size. In this limit, it should be clear that a particle entering the infinitesimal layer will leave it instantaneously, so that the net number of crossings at the layer is zero. This is illustrated in Fig. 3.1c. Accordingly, if we view the evolution of the Fokker-Planck equation as describing the behavior of an ensemble of particles, then the flux of particles across the boundary must be zero. Since this flux of particles is described by the current J_p, as defined in (2.9), it follows that $J_p = 0$ at the boundary.

This result can be obtained in other ways, e.g., by using the Skorokhod construction [20, 21] or by imposing a hard-wall potential force at the boundary, and implies mathematically that the relevant set of densities p on which the Fokker-Planck operator $\mathcal{L}^\dagger$ acts is the set of densities that satisfy

$$J_p(a^+) = J_p(b^-) = 0, \tag{3.3}$$

with the probability current $J_p(x)$ given from (2.9) as

$$J_p(x) = F(x)\,p(x) - \frac{\epsilon^2}{2}p'(x). \tag{3.4}$$

This defines the domain, $\mathcal{D}(\mathcal{L}^\dagger)$, of the Fokker-Planck operator $\mathcal{L}^\dagger$. In addition, we require a density $p \in \mathcal{D}(\mathcal{L}^\dagger)$ to be at least twice-differentiable given the nature of $\mathcal{L}^\dagger$ as a second-order differential operator. Furthermore $p \in \mathcal{D}(\mathcal{L}^\dagger)$ being a density requires that p is normalizeable and satisfies

$$\int_a^b p(x)\,dx < \infty. \tag{3.5}$$

Having determined what the boundary conditions are for the Fokker-Planck operator, we now derive the appropriate boundary conditions for the generator $\mathcal{L}$. Recall that the Fokker-Planck operator and the generator are adjoint operators with respect to the Lebesgue measure and are related via the natural inner product (2.15) for $p \in \mathcal{D}(\mathcal{L}^\dagger)$. Given that the operator $\mathcal{L}^\dagger$ is defined on normalized densities on $[a, b]$, the adjoint operator $\mathcal{L}$ is defined on those functions f on $[a, b]$ for which the inner product $\langle p, f\rangle$ is well-defined, meaning that

$$\langle p, f\rangle < \infty. \tag{3.6}$$

For the SDE (3.1) the Fokker-Planck operator $\mathcal{L}^\dagger$ is given from (2.6) as

$$\mathcal{L}^\dagger = -\frac{d}{dx}F + \frac{\epsilon^2}{2}\frac{d^2}{dx^2} \tag{3.7}$$

so that, similarly to our discussion in Chapter 2, we have

$$\begin{aligned}
\langle \mathcal{L}^\dagger p, f\rangle &= \int_a^b \left[-(Fp)'(x) + \frac{\epsilon^2}{2}p''(x)\right] f(x)\,dx \\
&= \left[-F(x)p(x)f(x) + \frac{\epsilon^2}{2}p'(x)f(x)\right]_a^b + \int_a^b \left[p(x)F(x) - \frac{\epsilon^2}{2}p'(x)\right] f'(x)\,dx \\
&= -f(x)J_p(x)\Big|_a^b - \frac{\epsilon^2}{2}p(x)f'(x)\Big|_a^b + \\
&\qquad + \int_a^b p(x)\left[F(x)\frac{d}{dx}f(x) + \frac{\epsilon^2}{2}\frac{d^2}{dx^2}f(x)\right] dx.
\end{aligned} \tag{3.8}$$

Given that p satisfies the zero current condition (3.3), we therefore have

$$\langle \mathcal{L}^\dagger p, f\rangle = -\frac{\epsilon^2}{2}p(x)f'(x)\Big|_a^b + \int_a^b p(x)\left[F(x)\frac{d}{dx}f(x) + \frac{\epsilon^2}{2}\frac{d^2}{dx^2}f(x)\right] dx. \tag{3.9}$$

From the definition (2.15), we thus see that $\mathcal{L}$ is only defined independently of any specific p if the condition

$$f'(a) = f'(b) = 0 \tag{3.10}$$

is satisfied for all f. In this case the generator $\mathcal{L}$ is given by

$$\mathcal{L} = F\frac{d}{dx} + \frac{\epsilon^2}{2}\frac{d^2}{dx^2} \tag{3.11}$$

which is the one-dimensional version of the expression given in (2.21). Condition (3.10) defines mathematically the domain, $\mathcal{D}(\mathcal{L})$, of $\mathcal{L}$. Clearly the functions in $\mathcal{D}(\mathcal{L})$ must also be at least twice-differentiable, given that $\mathcal{L}$ is a second-order differential operator.

In the next chapter, we will consider applications for which $b = \infty$. In this case, the normalization condition

$$\int_a^\infty p(x)\,dx < \infty \tag{3.12}$$

for $p \in \mathcal{D}(\mathcal{L}^\dagger)$ contrains p to decay to 0 as $x \to \infty$, while a zero-current condition at ∞ is required to ensure that there is no 'flow' of probability at ∞, so that probability is conserved. From the expression (3.4) for the current, along with the fact that p decays to 0 as $x \to \infty$, we must therefore also have that p' tends to 0 as $x \to \infty$. For

$$\frac{\epsilon^2}{2}p(x)f'(x)\Big|_a^\infty = 0 \tag{3.13}$$

to hold, which is necessary for $\mathcal{L}$ to be defined unambiguously (refer to (3.9)), we need only require $f'(a) = 0$ since p decays to 0 as $x \to \infty$. The case where $a = -\infty$ and b is finite is treated in a similar fashion.

3.2.1 Example: Reflected Brownian Motion with Drift

As an illustration of the boundary conditions just obtained, we consider the process X_t satisfying the SDE

$$dX_t = -\mu\,dt + \epsilon\,dW_t \tag{3.14}$$

with $\mu > 0$ and $X_t \in [0, \infty)$ with reflection at $x = 0$. This process is known as reflected Brownian motion with drift. The Fokker-Planck operator associated with this process is given by

$$\mathcal{L}^\dagger = \mu\frac{d}{dx} + \frac{\epsilon^2}{2}\frac{d^2}{dx^2}, \tag{3.15}$$

and acts on densities p satisfying the zero-current condition $J_p(0^+) = 0$ which for the force $F(x) = -\mu$ becomes

$$\left[-\mu p(x) - \frac{\epsilon^2}{2}p'(x)\right]_{x=0^+} = 0, \tag{3.16}$$

or more explicitly

$$p'(0^+) = -\frac{2\mu}{\epsilon^2}\,p(0^+) \tag{3.17}$$

This type of boundary condition, involving both the function p and its derivative p', is known as a *Robin* or *mixed boundary condition*.

The stationary density p^* is found as the density which satisfies $\mathcal{L}^\dagger p^* = 0$ along with the boundary condition (3.17). The solution is found to be a Gibbs density and is given from (2.13) as

$$p^*(x) = \frac{2\mu}{\epsilon^2}\exp\left[-\frac{2\mu\,x}{\epsilon^2}\right], \quad x \geq 0, \tag{3.18}$$

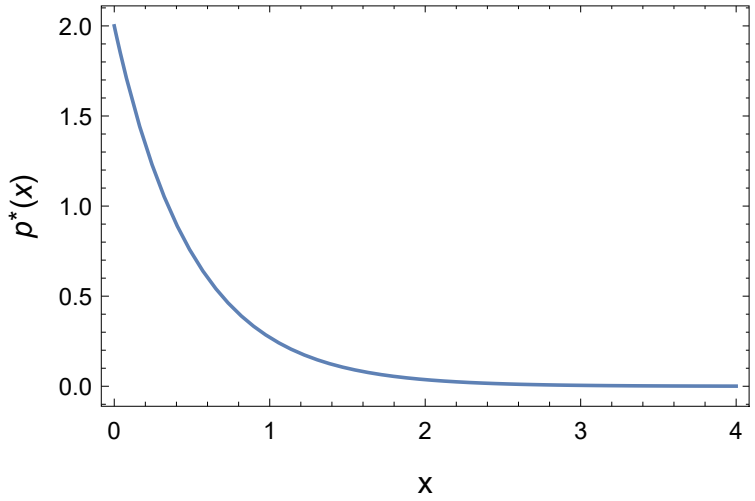

Figure 3.2: Stationary density p^* for reflected Brownian motion with drift. Parameters: $\mu = 1$ and $\epsilon = 1$.

where we have properly normalized p^*. The stationary density is shown in Fig. 3.2. Note that Brownian motion on $\mathbb{R}$ (with or without drift) has no stationary distribution. The fact that reflected Brownian motion with drift has one is due to the presence of the reflecting wall and the negative drift which serves to confine the motion close to the origin. Note also that because X_t is one-dimensional, and $J = 0$ at $x = 0$, then we must have that $J = 0$ everywhere for the density p^* to be stationary. If the current was non-zero anywhere there would be a net flow of probability and the density would not be time-independent.

For future use, note that the generator $\mathcal{L}$ is given from (3.11) by

$$\mathcal{L} = -\mu \frac{d}{dx} + \frac{\epsilon^2}{2} \frac{d^2}{dx^2} \tag{3.19}$$

and acts on test functions f satisfying $f'(0^+) = 0$ according to (3.10).

3.2.2 Example: Positive Ornstein-Uhlenbeck Process with Reflection

We now consider the Ornstein-Uhlenbeck process satisfying the SDE (2.47) with X_t constrained to take values in $[0, \infty)$ and $x = 0$ considered to be a reflecting boundary. As before for the normal Ornstein-Uhlenbeck process, $x = \infty$ is a natural boundary in the sense of the Feller classification.

The Fokker-Planck operator associated with this process is given by

$$\mathcal{L}^\dagger = \gamma \frac{d}{dx} x + \frac{\epsilon^2}{2} \frac{d^2}{dx^2} \tag{3.20}$$

and acts on densities p satisfying the zero current condition $J_p(0^+) = 0$, yielding

$$\left[-\gamma x p(x) - \frac{\epsilon^2}{2} p'(x) \right]_{x=0^+} = 0 \tag{3.21}$$

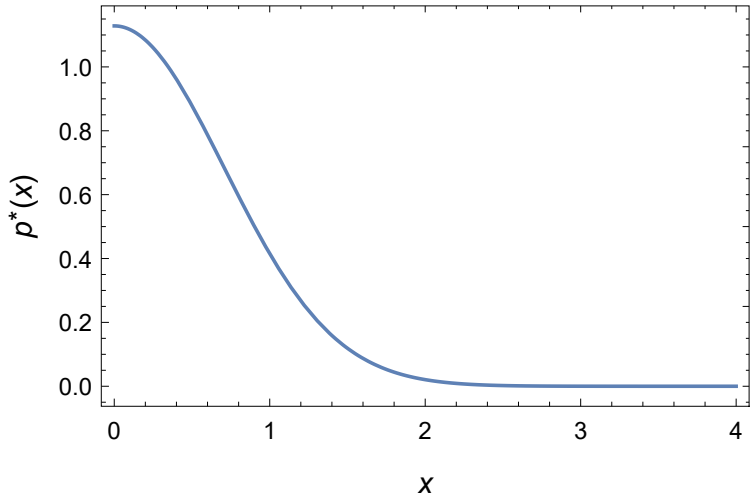

Figure 3.3: Stationary density p^* for the reflected Ornstein-Uhlenbeck process with parameters $\gamma = 1$ and $\epsilon = 1$.

and therefore $p'(0^+) = 0$. The stationary density p^* that satisfies $\mathcal{L}^\dagger p^* = 0$ while being subject to the condition $p'(0^+) = 0$ is given by

$$p^*(x) = 2\sqrt{\frac{\gamma}{\pi\epsilon^2}} \exp\left[-\frac{\gamma x^2}{\epsilon^2}\right], \quad x \geq 0. \tag{3.22}$$

This Gibbs density associated with the process is simply the density found for the normal Ornstein-Uhlenbeck process in (2.49) truncated on $x \geq 0$ and therefore having a different normalization factor. The stationary density is shown in Fig. 3.3.

The generator $\mathcal{L}$ of the process is given from (3.11) by

$$\mathcal{L} = -\gamma x \frac{d}{dx} + \frac{\epsilon^2}{2}\frac{d^2}{dx^2} \tag{3.23}$$

and, as before, acts on test functions f for which $f'(0^+) = 0$.

3.3 Large Deviations

We come now to the main problem of the thesis which is to explain how large deviations of reflected diffusions are obtained. Following the paper by Fatalov [35] mentioned in the introduction, which considers the large deviations of the area of reflected Brownian motion with negative drift, we extend that paper by considering more general diffusions, by explaining in detail how to implement reflecting boundary conditions in the spectral problem defining the SCGF, and by applying these results to the driven process.

We consider, as before, a diffusion X_t satisfying an SDE of the form (3.1) and a time-integrated observable A_T of the form considered in Chapter 2. We

are interested in obtaining the SCGF $\lambda(k)$ associated with the observable A_T. We recall that $\lambda(k)$ is found as the dominant eigenvalue of the spectral problem given by

$$\mathcal{L}_k r_k^{(n)}(x) = \lambda_n(k) r_k^{(n)}(x) \tag{3.24}$$

and the adjoint equation

$$\mathcal{L}_k^\dagger l_k^{(n)}(x) = \lambda_n(k) l_k^{(n)}(x), \tag{3.25}$$

where $\mathcal{L}_k$ is the tilted generator having the form

$$\mathcal{L}_k = \mathcal{L} + kf \tag{3.26}$$

with $\mathcal{L}$ the generator of the process X_t. The index n labels the different eigenvalues and eigenfunctions for the spectral problem at hand. As before, the operators $\mathcal{L}_k$ and $\mathcal{L}_k^\dagger$ are viewed as adjoints with respect to the inner product (2.15). The eigenfunctions $r_k^{(n)}$ and $l_k^{(n)}$ are thus required to satisfy

$$\langle l_k^{(n)}, r_k^{(n)} \rangle < \infty \tag{3.27}$$

Here, we choose the eigenfunctions in such a manner that the normalization condition

$$\langle l_k^{(n)}, r_k^{(n)} \rangle = 1 \tag{3.28}$$

holds. This normalization condition only fixes the normalization of the product $l_k^{(n)} r_k^{(n)}$, not the eigenfunctions individually. We therefore also require that

$$\int_a^b l_k^{(n)}\, dx = 1, \tag{3.29}$$

which fixes the normalization for both $l_k^{(n)}$ and $r_k^{(n)}$. This integrability condition is natural given the relation of the operator $\mathcal{L}_k^\dagger$ to the Fokker-Planck operator, to which it must correspond in the case $k = 0$.

Proceeding, we note that since

$$\langle \mathcal{L}_k^\dagger l_k^{(i)}, r_k^{(j)} \rangle = \langle l_k^{(i)}, \mathcal{L}_k r_k^{(j)} \rangle \tag{3.30}$$

from the definition of the adjoint and

$$\lambda_i(k) \langle l_k^{(i)}, r_k^{(j)} \rangle = \langle \mathcal{L}_k^\dagger l_k^{(i)}, r_k^{(j)} \rangle = \langle l_k^{(i)}, \mathcal{L}_k r_k^{(j)} \rangle = \lambda_j(k) \langle l_k^{(i)}, r_k^{(j)} \rangle \tag{3.31}$$

we must have that

$$\langle l_k^{(i)}, r_k^{(j)} \rangle = 0 \quad \text{for} \quad i \neq j. \tag{3.32}$$

Combining this with the normalization condition (3.28) we obtain

$$\langle l_k^{(i)}, r_k^{(j)} \rangle = \delta_{i,j} \tag{3.33}$$

for the eigenfunctions.

We now need to determine the appropriate boundary conditions applied to the eigenfunctions of the operator $\mathcal{L}_k$ and its adjoint $\mathcal{L}_k^\dagger$ in order to fully determine the spectrum of these operators. The central observation in determining these boundary conditions is that the operators $\mathcal{L}_k$ and $\mathcal{L}_k^\dagger$ are parameter extensions (involving the parameter k) of the operators $\mathcal{L}$ and $\mathcal{L}^\dagger$, respectively, satisfying $\mathcal{L}_{k=0} = \mathcal{L}$ and $\mathcal{L}_{k=0}^\dagger = \mathcal{L}^\dagger$, so that the boundary conditions placed on these operators must be independent of k. Consequently, the operators $\mathcal{L}_k^\dagger$ and $\mathcal{L}_k$ must inherit the boundary conditions of $\mathcal{L}^\dagger$ and $\mathcal{L}$, respectively. For $\mathcal{L}_k^\dagger$ this means explicitly that the set of eigenfunctions $l_k^{(n)}$ satisfy the zero current condition

$$J_{l_k^{(n)}}(x)\Big|_{x=a^+} = J_{l_k^{(n)}}(x)\Big|_{x=b^-} = 0, \tag{3.34}$$

which can be stated explicitly as

$$F(a^+)\, l_k^{(n)}(a^+) = \frac{\epsilon^2}{2}\frac{dl_k^{(n)}(x)}{dx}\Big|_{x=a^+} \quad \text{and} \quad F(b^-)\, l_k^{(n)}(b^-) = \frac{\epsilon^2}{2}\frac{dl_k^{(n)}(x)}{dx}\Big|_{x=b^-}. \tag{3.35}$$

As for the set of eigenfunctions $r_k^{(n)}$ associated with $\mathcal{L}_k$, they inherit the boundary condition (3.10) and therefore satisfy

$$\frac{dr_k^{(n)}(x)}{dx}\Big|_{x=a^+} = \frac{dr_k^{(n)}(x)}{dx}\Big|_{x=b^-} = 0. \tag{3.36}$$

The boundary conditions for $\mathcal{L}_k$ can also be found, as before, by considering the definition of the adjoint (3.30) and taking into account the boundary conditions for the eigenfunctions $l_k^{(n)}$. The calculations involved are identical to the procedure followed in (3.8). A similar argument can be made for obtaining the boundary conditions for $l_k^{(n)}$ using (3.36) as a starting point.

3.4 Driven Process and Reflecting Boundaries

We now look at the consequences of the boundary conditions for $r_k^{(n)}$ and $l_k^{(n)}$ for the driven process. First we note from the boundary conditions (3.34) and (3.36) that

$$r_k^{(n)}(x) J_{l_k^{(n)}}(x)\Big|_{x=a^+} = r_k^{(n)}(x) J_{l_k^{(n)}}(x)\Big|_{x=b^-} = 0 \tag{3.37}$$

and

$$\frac{\epsilon^2}{2} l_k^{(n)}(x)\frac{dr_k^{(n)}(x)}{dx}\Big|_{x=a^+} = \frac{\epsilon^2}{2} l_k^{(n)}(x)\frac{dr_k^{(n)}(x)}{dx}\Big|_{x=b^-} = 0. \tag{3.38}$$

We recognize these as the boundary terms arising in (3.8) due to integration by parts where $l_k^{(n)}$ and $r_k^{(n)}$ here play the parts of p and f (respectively) in (3.8).

In particular, we note that upon combining (3.37) and (3.38) we have

$$\left[r_k^{(n)}(x)J_{l_k^{(n)}}(x) - \frac{\epsilon^2}{2}l_k^{(n)}(x)\frac{dr_k^{(n)}(x)}{dx}\right]_{x=a^+} = 0 \tag{3.39}$$

with an identical equation holding for $x = b^-$. Expanding the expression for the current associated with $l_k^{(n)}$ yields

$$\left[F(x)r_k^{(n)}(x)l_k^{(n)}(x) - \frac{\epsilon^2}{2}r_k^{(n)}(x)\frac{dl_k^{(n)}(x)}{dx} - \frac{\epsilon^2}{2}l_k^{(n)}(x)\frac{dr_k^{(n)}(x)}{dx}\right]_{x=a^+} = 0 \tag{3.40}$$

which reduces to

$$\left[F(x)\left(r_k^{(n)}(x)l_k^{(n)}(x)\right) - \frac{\epsilon^2}{2}\frac{d}{dx}\left(r_k^{(n)}(x)l_k^{(n)}(x)\right)\right]_{x=a^+} = J_{r_k^{(n)}l_k^{(n)}}(x)\Big|_{x=a^+} = 0 \tag{3.41}$$

with an identical expression holding for $x = b^-$. This shows interestingly that the combination $r_k^{(n)}l_k^{(n)}$ also satisfies a zero current condition at the boundaries. This makes sense given that $p_k = r_k\, l_k$ is the stationary distribution associated with the driven process $X_t^{(k)}$. The driven process corresponds asymptotically to the process X_t conditioned on obtaining a given a fluctuation and so still retains the zero current condition at the boundaries.

From these results, we can draw a few more interesting conclusions for behavior of the driven force F_k. As we have seen, the eigenfunctions $r_k^{(n)}$ satisfy the boundary condition (3.36). In particular we have $r_k'(a^+) = r_k'(b^-) = 0$ for the dominant eigenfunction r_k. We recall from the definition of the driven force F_k given in (2.77) that it differs from the force $F(x)$ only by a term depending on $r_k'(x)$. We find that since this term is zero at the boundaries, by (2.77), the driven force therefore satisfies

$$F_k(a^+) = F(a^+) \quad \text{and} \quad F_k(b^-) = F(b^-). \tag{3.42}$$

In other words, the driven force is the same as the original force at the reflecting boundaries. For the driven current $J_p^{(k)}$ associated with the effective process $X_t^{(k)}$ having drift F_k, defined in the usual manner as

$$J_p^{(k)}(x) = F_k(x)p(x) - \frac{\epsilon^2}{2}\frac{d}{dx}p(x) \tag{3.43}$$

this implies that at the boundaries, where the driven force is the same as the original force, we obtain

$$J_p^{(k)}(a^+) = J_p(a^+) = 0 \quad \text{and} \quad J_p^{(k)}(b^-) = J_p(b^-) = 0 \tag{3.44}$$

for any function p that satisfies a zero current condition for the current J associated with the original process. This includes, as we have seen, the eigenfunctions $l_k^{(n)}$ as well as combinations of the form $r_k^{(n)}l_k^{(n)}$. In particular we have that $J_{p_k}^{(k)}$ is

zero at the boundaries. This means that the current associated with the driven force F_k and the stationary distribution of the driven process also satisfies a zero current condition at the boundaries, as one would expect for a system having reflecting boundary conditions.

In conclusion, the driven force at the boundaries is the same as the original force F and the driven current $J_{p_k}^{(k)}$ satisfies a zero current condition at the boundaries as for $k = 0$.

3.5 Boundary Conditions for the Symmetrized Problem

In Chapter 2 we saw that, while the tilted generator $\mathcal{L}_k$ is typically not Hermitian, we could symmetrize the spectral problem in the case where $\mathcal{L}_k$ has a real spectrum. In this case, the spectral problem reduces to the study of a Hermitian operator $\mathcal{H}_k$. We now discuss the boundary conditions for this Hermitian (symmetrized) operator $\mathcal{H}_k$ given by

$$\mathcal{H}_k = (p^*)^{1/2}\mathcal{L}_k(p^*)^{-1/2}, \tag{3.45}$$

which has the same spectrum $\lambda_n(k)$ as $\mathcal{L}_k$ and has eigenfunctions $\psi_k^{(n)}$ which satisfy the relations (2.45) and therefore

$$\psi_k^{(n)}(x)^2 = r_k^{(n)}(x)l_k^{(n)}(x). \tag{3.46}$$

From (3.41) we have that the eigenfunctions $\psi_k^{(n)}$ thus satisfy the boundary condition

$$J_{\left(\psi_k^{(n)}\right)^2}(x)\Big|_{x=a^+} = J_{\left(\psi_k^{(n)}\right)^2}(x)\Big|_{x=b^-} = 0. \tag{3.47}$$

This means explicitly that we have

$$J_{\left(\psi_k^{(n)}\right)^2}(x) = \left[F(x)\left(\psi_k^{(n)}(x)\right)^2 - \frac{\epsilon^2}{2}\frac{d}{dx}\left(\psi_k^{(n)}(x)\right)^2\right] \tag{3.48}$$

and so we have

$$\psi_k^{(n)\prime}(a^+) = \frac{F(a^+)}{\epsilon^2}\psi_k^{(n)}(a^+) \quad \text{and} \quad \psi_k^{(n)\prime}(b^-) = \frac{F(b^-)}{\epsilon^2}\psi_k^{(n)}(b^-) \tag{3.49}$$

for the eigenfunctions $\psi_k^{(n)}$. Finally, given that the eigenfunctions $l_k^{(n)}$ and $r_k^{(n)}$ form an orthonormal basis, following eq. 3.33, we also find that

$$\langle l_k^{(i)}, r_k^{(j)}\rangle = \int_a^b \psi_k^{(i)}(x)\,\psi_k^{(j)}(x)\,dx = \delta_{i,j}. \tag{3.50}$$

We can therefore regard the eigenfunctions $\psi_k^{(n)}$ as square-integrable, orthonormal eigenfunctions satisfying the Robin (mixed) boundary conditions (3.49) in a quantum problem. As before we can generalize all results here very easily to the case where only one of a, b is finite.

Chapter 4

Applications

We illustrate in this chapter the results obtained in Chapter 3 by applying them to two examples already seen in Chapter 3, namely, the reflected Ornstein-Uhlenbeck process and reflected Brownian motion with dirft. Each of these two systems can be solved exactly and give rise to interesting properties for the driven process in the presence of a reflecting boundary.

4.1 Reflected Ornstein-Uhlenbeck Process with Linear Observable

The first system that we study is the reflected Ornstein-Uhlenbeck process in one dimension, introduced in Section 3.2.2. As discussed previously, reflecting boundary conditions will be implemented at the level of the Fokker-Planck operator $\mathcal{L}^\dagger$ by requiring that the current $J_p(x)$ associated with this process satisfies

$$J_p(x)\Big|_{x=0^+} = 0 \tag{4.1}$$

for all p in the domain of $\mathcal{L}^\dagger$. As discussed in Section 3.2.2, for the process under consideration, this condition on the current reduces to the Neumann boundary condition $p'(0^+) = 0$. The SDE (2.47) is gradient with the stationary Gibbs density (3.22) satisfying this boundary condition at $x = 0$.

4.1.1 Spectral Problem for Linear Observable

The observable A_T that we consider here is the same as that considered in Section 2.7.1, namely,

$$A_T = \frac{1}{T}\int_0^T X_t\, dt \tag{4.2}$$

and leads to the tilted generator $\mathcal{L}_k$ given before in (2.51). As before, in the treatment of the Ornstein-Uhlenbeck process with linear observable, we will obtain

the SCGF by solving the spectral problem associated with the symmetrized operator $\mathcal{H}_k$, where we note that this operator is now only symmetrized for $x > 0$. Since the stationary distribution p^* given in (3.22) for the reflected Ornstein-Uhlenbeck process has the same form as that of the normal Ornstein-Uhlenbeck process, we have that the symmetrized operator $\mathcal{H}_k$ has the same form as in (2.52) on $x \geq 0$. The eigenfunctions $\psi_k^{(n)}$ must therefore satisfy the differential equation (2.53) with the difference here being that these eigenfunctions are now restricted to $x \geq 0$ and required to satisfy the boundary condition (3.49) at $x = 0^+$, which, for the force $F(x) = -\gamma x$, reduces to

$$\psi_k^{(n)\prime}(0) = 0 \tag{4.3}$$

along with the usual normalization condition

$$\int_0^\infty \psi_k^{(n)}(x)^2 \, dx = 1 \tag{4.4}$$

which requires that

$$\lim_{x\to\infty} \psi_k^{(n)}(x)^2 = 0. \tag{4.5}$$

The solutions $\psi_k^{(n)}$ to the differential equation (2.53) belong to the class of functions known as parabolic cylinder functions. A special class of the parabolic cylinder functions are related to the Hermite polynomials that we are familiar with from quantum mechanics. More precisely, we have that $\psi_k^{(n)}$ has the form

$$\psi_k^{(n)}(x) = D_{\xi_n}\left(\frac{\sqrt{2\gamma}x}{\epsilon} - \frac{\sqrt{2}k\epsilon}{\gamma^{3/2}}\right), \tag{4.6}$$

where we have defined

$$\xi_n = \frac{k^2\epsilon^2 - 2\gamma^2\lambda_n(k)}{2\gamma^3} \tag{4.7}$$

and where $D_\nu(z)$ indicates a parabolic cylinder function. Valid solutions to the spectral problem under consideration must further satisfy the boundary condition (4.3) which constrains possible values of $\lambda_n(k)$. Upon substituting the form (4.6) for the eigenfunctions into the boundary condition (4.3), we obtain the transcendental equation

$$\frac{k\epsilon}{\sqrt{2}\gamma^{3/2}} D_{\xi_n}\left(-\frac{\sqrt{2}k\epsilon}{\gamma^{3/2}}\right) + D_{\xi_n+1}\left(\frac{\sqrt{2}k\epsilon}{\gamma^{3/2}}\right) = 0 \tag{4.8}$$

which is only satisfied for valid eigenvalues λ_n. In deriving this equation, we have used the identities

$$D_\nu'(z) + \frac{1}{2}zD_\nu(z) - \nu D_{\nu-1}(z) = 0 \tag{4.9}$$

and

$$D_{\nu+1}(z) - zD_\nu(z) + \nu D_{\nu-1}(z) = 0 \tag{4.10}$$

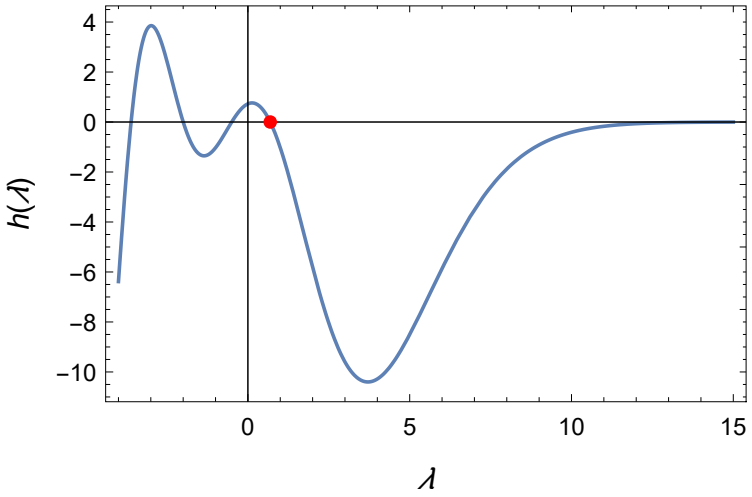

Figure 4.1: Function $h(\lambda)$ defined in (4.11) for the values $\epsilon = 1$, $\gamma = 1$ and $k = 1$. The red dot indicates the maximal zero of $h(\lambda)$ corresponding to the maximal eigenvalue (SCGF) of the spectral problem for this set of parameters.

for the parabolic cylinder functions $D_\nu(z)$. Thus we see that the eigenvalues $\lambda_n(k)$ for our spectral problem are found as the zeroes of the function $h(\lambda)$ given by

$$h(\lambda) = \frac{k\epsilon}{\sqrt{2}\gamma^{3/2}} D_\xi\left(-\frac{\sqrt{2}k\epsilon}{\gamma^{3/2}}\right) + D_{\xi+1}\left(\frac{\sqrt{2}k\epsilon}{\gamma^{3/2}}\right), \tag{4.11}$$

with $\xi = (k^2\epsilon^2 - 2\gamma^2\lambda)/2\gamma^3$.

A plot of the function $h(\lambda)$ for a specific set of the parameters ϵ, γ and k is shown in Fig. 4.1. Each zero corresponds to a different eigenvalue, with the largest (shown with a dot) corresponding to the SCGF.

We can now obtain the roots of $h(\lambda)$ for a given set of parameters ϵ and γ while varying the value of k to obtain the eigenvalues $\lambda_n(k)$ as functions of k via interpolation. This allows us to find the SCGF $\lambda(k)$, the maximal eigenvalue, as a function of k for a given set of paramaters. The result of this procedure is shown in Fig. 4.2. We note from this that we have $\lambda(0) = 0$, which is a general property of the SCGF. Furthermore, using the relation $\lambda'(k) = a(k)$, we have $\lambda'(-\infty) = 0$, as a result of the fact that the lower bound of A_T is 0, so that the SCGF becomes asymptotically linear as $k \to -\infty$. In the same manner, we have $\lambda'(\infty) = \infty$ since A_T is unbounded from above. These properties can be seen in Fig. 4.2.

Since the SCGF is differentiable and strictly convex we obtain the rate function $I(a)$ as the Legendre transform of $\lambda(k)$, according to the Gärtner-Ellis theorem. The result is shown in Fig. 4.3. We see that $I(a)$ is defined only for $a \geq 0$, since A_T is now non-negative due to the reflection. Moreover $I(a)$ is convex, tends asymptotically to ∞ as $a \to 0$, and has a unique minimum and zero a^* corresponding, as we know, to the large time expectation and typical value

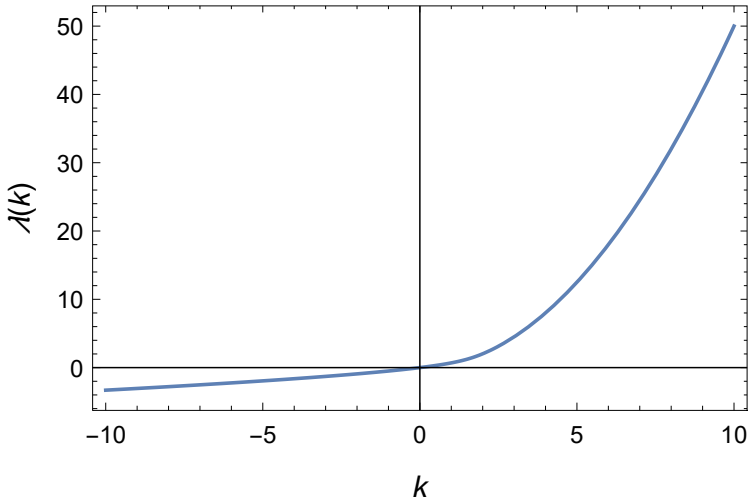

Figure 4.2: SCGF $\lambda(k)$ for the linear observable of the reflected Ornstein-Uhlenbeck process with parameters $\epsilon = 1$ and $\gamma = 1$.

of A_T. Given that the process under consideration is ergodic, the value a^* is found by calculating the expectation of $f(x) = x$ with respect to the stationary distribution p^*, given by (3.22), of the process. We therefore obtain

$$a^* = \int_0^\infty x\, p^*(x)\, dx = 2\sqrt{\frac{\gamma}{\pi\epsilon^2}} \int_0^\infty x \exp\left[-\frac{\gamma x^2}{\epsilon^2}\right] dx. \tag{4.12}$$

By performing the Gaussian integral in (4.12) the value of a^* is found to be

$$a^* = \sqrt{\frac{\epsilon^2}{\pi\gamma}}. \tag{4.13}$$

For the values $\epsilon, \gamma = 1$ we have $a^* = 1/\sqrt{\pi} \approx 0.564$, which is corroborated in Fig. 4.3.

We now consider the driven process $X_t^{(k)}$ with driven force F_k that manifests the fluctuation $a(k) = \lambda'(k)$ corresponding to k. The driven force F_k and its corresponding driven potential U_k can be obtained by substituting our expression for $\psi_k = \psi_k^{(0)}$ given from (4.6) into the relations (2.81) and (2.82). We use a non-normalized ψ_k, since the normalization constant cancels out in the expression for F_k and it is sufficient to define U_k up to a constant. This leads to

$$F_k(x) = \epsilon^2 \frac{\psi_k'(x)}{\psi_k(x)} = \sqrt{2}\gamma\epsilon \frac{D'_{\xi(k)}\left(\frac{\sqrt{2\gamma}x}{\epsilon} - \frac{\sqrt{2}k\epsilon}{\gamma^{3/2}}\right)}{D_{\xi(k)}\left(\frac{\sqrt{2\gamma}x}{\epsilon} - \frac{\sqrt{2}k\epsilon}{\gamma^{3/2}}\right)}, \tag{4.14}$$

which becomes

$$F_k(x) = \sqrt{2}\gamma\epsilon \frac{\frac{1}{2}\left(\frac{\sqrt{2\gamma}x}{\epsilon} - \frac{\sqrt{2}k\epsilon}{\gamma^{3/2}}\right) D_{\xi(k)}\left(\frac{\sqrt{2\gamma}x}{\epsilon} - \frac{\sqrt{2}k\epsilon}{\gamma^{3/2}}\right) - D_{\xi(k)+1}\left(\frac{\sqrt{2\gamma}x}{\epsilon} - \frac{\sqrt{2}k\epsilon}{\gamma^{3/2}}\right)}{D_{\xi(k)}\left(\frac{\sqrt{2\gamma}x}{\epsilon} - \frac{\sqrt{2}k\epsilon}{\gamma^{3/2}}\right)} \tag{4.15}$$

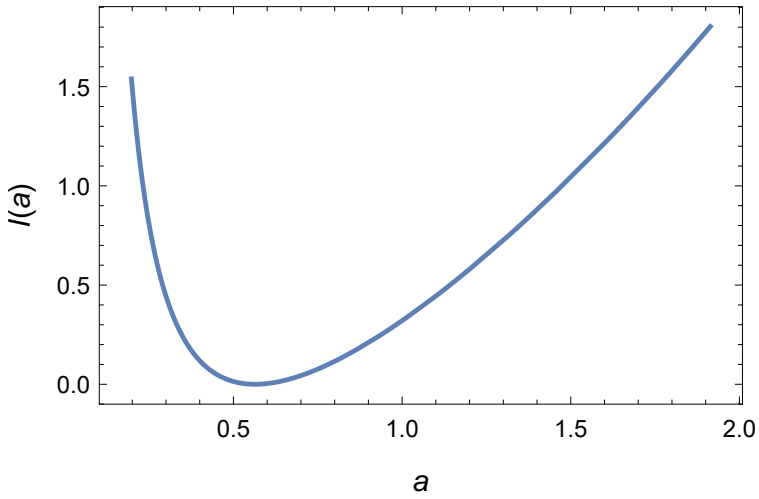

Figure 4.3: Rate function $I(a)$ for the linear observable of the reflected Ornstein-Uhlenbeck process with parameters $\epsilon = 1$ and $\gamma = 1$.

upon using the relations (4.9) and (4.10) for the parabolic cylinder functions. For U_k we have

$$U_k(x) = -\epsilon^2 \ln\left(\psi_k(x)\right) = -\epsilon^2 \ln\left[D_{\xi(k)}\left(\frac{\sqrt{2\gamma}x}{\epsilon} - \frac{\sqrt{2}k\epsilon}{\gamma^{3/2}}\right)\right], \tag{4.16}$$

where as before,

$$\xi(k) = \frac{k^2\epsilon^2 - 2\gamma^2\lambda(k)}{2\gamma^3}. \tag{4.17}$$

We observe from Fig. 4.4 that we have $F_k(0) = F(0) = 0$ in accordance with our discussion in Section 3.4. Furthermore, we note that there are two qualitatively distinct cases for the behavior of the driven force F_k – the case with $k < 0$ and the case with $k > 0$. For $k < 0$ we observe that F_k has a single zero at $x = 0$, while for $k > 0$ there is an additional zero, around which F_k is approximately linear with slope $-\gamma$. As can be seen from Fig. 4.4 this implies that, for $k < 0$, we have that the effective potential U_k has a minimum at $x = 0$, while for $k > 0$, the location of the minimum of U_k shifts to the right as k increases. This in turn implies that the Gibbs density p_k has a maximum at $x = 0$ for $k < 0$, with its maximum shifted away from $x = 0$ for increasing $k > 0$. This can be seen in Fig. 4.6. Further, in plotting $\lambda'(k)$ in Fig. 4.5, which represents the fluctuation $a(k)$ corresponding to a given value of k, we observe that these two cases are responsible for two different branches of the rate function I. We have that the $k < 0$ branch creates fluctuations $a < a^*$, while the $k > 0$ branch is responsible for fluctuations $a > a^*$, with a^* being the zero of the rate function $I(a^*) = 0$.

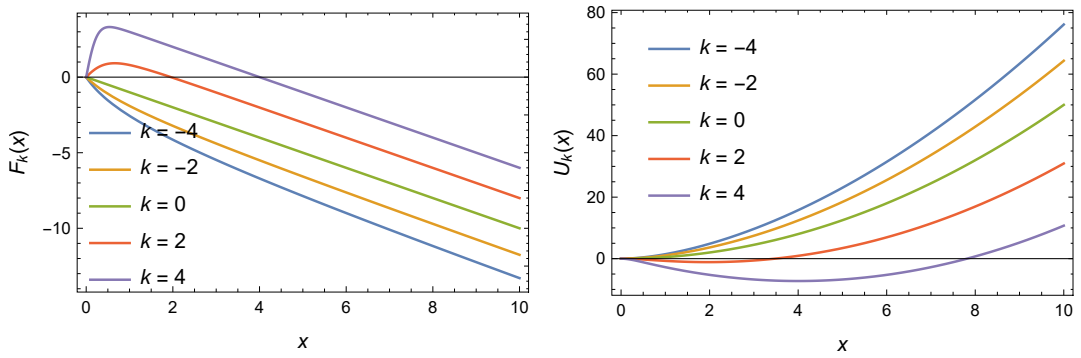

Figure 4.4: Left: Driven force $F_k(x)$ for various values of k. Right: Driven potential $U_k(x)$ for those same values of k. In both cases, we have used the parameters $\epsilon = 1$ and $\gamma = 1$.

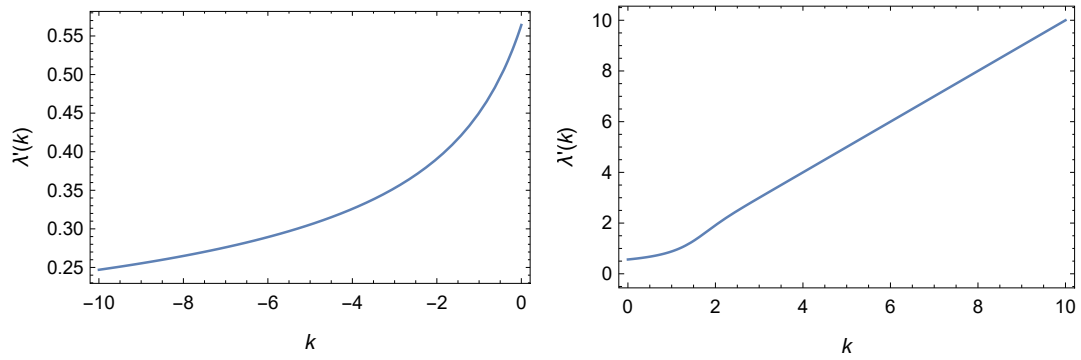

Figure 4.5: Left: Values for the fluctuation $a(k) = \lambda'(k)$ for the case where $k < 0$. Right: Values for the fluctuation $a(k) = \lambda'(k)$ for the case where $k > 0$. Parameter values of $\epsilon = 1$ and $\gamma = 1$ are used.

4.1.2 Approximation of the Driven Process

We now wish to provide an approximation of the driven force F_k to gain some insight into the essential features of this driven force. An approximate force $\tilde{F}_k$ will accomplish this if it is simpler than the true driven force yet nevertheless models important features of the problem at hand with sufficient accuracy.

It is shown in [51] that the rate function $I(a)$ can be regarded as the solution to the constrained optimization problem

$$I(a) = \inf_{u:\tilde{A}(u)=a} \frac{1}{2\epsilon^2} \int_0^\infty \big(F(x) - u(x)\big)^2 p_u^*(x)\, dx \tag{4.18}$$

where F is the drift for the process X_t under consideration, p_u^* is the invariant (stationary) distribution associated with the drift u and for a functional A_T we have

$$\tilde{A}(u) = \int_0^\infty f(x) p_u^*(x)\, dx, \tag{4.19}$$

which represents the long-time value of the functional A_T for a process with u as its drift. In our current case, we have $F(x) = -\gamma x$ and $f(x) = x$ since we are considering a linear observable. It is shown in [51] that the function u that serves as the true minimizer in (4.18) is the actual driven force F_k.

Based on this result we can construct an approximate force $\tilde{F}_b(x)$ parametrized by some variable b to which there corresponds an approximation $\tilde{I}$ of the rate function I given by

$$\tilde{I}(\tilde{a}_b) = \frac{1}{2\epsilon^2} \int_0^\infty \left(F(x) - \tilde{F}_b(x)\right)^2 \tilde{p}_b(x)\, dx \tag{4.20}$$

where $\tilde{p}_b$ is the invariant (stationary) density associated with the drift $\tilde{F}_b$ and $\tilde{a}_b$ is the long-time value of the functional A_T for a process having $\tilde{F}_b$ as its drift:

$$\tilde{a}_b = \int_0^\infty x\, \tilde{p}_b(x)\, dx. \tag{4.21}$$

The validity of the approximation is determined by the extent to which the approximate force $\tilde{F}_b$ resembles the true driven force F_k for the same value of the observable.

From the definition (4.18), we see that for any a we must have $\tilde{I}(a) \geq I(a)$ given that I can be viewed as the infimum over all possible $\tilde{I}$. It is also clear from the expressions (4.18) and (4.20) that we must simultaneously consider the form of both the approximate force and the invariant distribution associated with it. The invariant distribution acts as a weight in the integrals (4.18) and (4.20) and therefore values of x for which the invariant distribution is negligible will not contribute to these integrals in a significant manner. It is therefore important that the $\tilde{F}$ we choose as an approximation should model the true driven force F_k closely for those values of x that maximize the true invariant distribution p_k, since these values will contribute the most to the integral (4.18). In order to construct a good approximation we must therefore understand the structure of the invariant distribution $p_k = \psi_k^2$ associated with the driven force F_k.

As noted previously, the driven force F_k shown in Fig. 4.4 has qualitatively different behavior for the cases $k < 0$ and $k > 0$. We will therefore treat these cases separately, starting with $k < 0$. From Fig. 4.6 we observe that for $k < 0$ the invariant distribution p_k attains its maximum at $x = 0$ and decays rapidly to 0 as x increases. The approximate force $\tilde{F}$ that we choose must therefore model F_k accurately close to $x = 0$. The simplest such approximation, suggested from the form of F_k shown in Fig. 4.4, is a linear force $\tilde{F}_b$ depending on the parameter b as

$$\tilde{F}_b(x) = -bx, \quad b > \gamma. \tag{4.22}$$

Only $b > -\gamma$ need be considered since it is clear from Fig. 4.4 that $F_k'(0) < \gamma$ for $k < 0$. Essentially, the approximation (4.22) is a first-order Taylor expansion around $x = 0$ of the driven force F_k which establishes a one-to-one relationship between b and k in the sense that to each k there corresponds a $b(k)$ such that $F_k'(0) = -b(k)$, and vice versa.

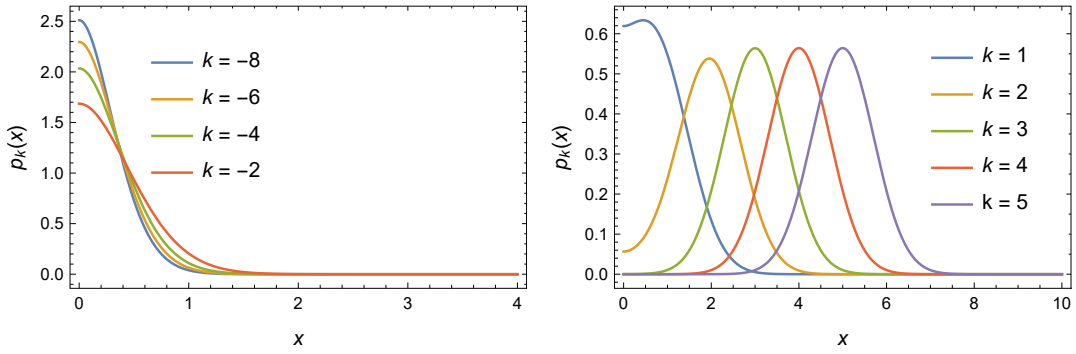

Figure 4.6: Invariant densities p_k for the reflected Ornstein-Uhlenbeck process. Left: p_k shown for different values $k < 0$. Right: p_k shown for different values $k > 0$. Parameter values of $\epsilon = 1$ and $\gamma = 1$ are used.

In order to obtain the quantities $\tilde{a}_b$ and $\tilde{I}(\tilde{a}_b)$ as in (4.21) and (4.20) we must calculate the invariant distribution $\tilde{p}_b$ associated with our force $\tilde{F}_b$. This is found in the usual manner as the Gibbs density associated with the drift $\tilde{F}_b$. Corresponding to the force $\tilde{F}_b$ we have the potential $\tilde{U}_b$ which satisfies $\tilde{U}_b'(x) = -\tilde{F}_b(x)$, so that

$$\tilde{U}_b(x) = \frac{bx^2}{2}. \tag{4.23}$$

The Gibbs density associated with this potential is therefore

$$\tilde{p}_b(x) = \mathcal{N} \exp\left[-\frac{2\tilde{U}_b(x)}{\epsilon^2}\right] = 2\sqrt{\frac{b}{\pi\epsilon^2}} \exp\left[-\frac{bx^2}{\epsilon^2}\right] \tag{4.24}$$

for $x \geq 0$, where we have properly normalized the density $\tilde{p}_b$. To find $\tilde{a}_b$ we now have from (4.21) that

$$\tilde{a}_b = \int_0^\infty x\, \tilde{p}_b(x)\, dx = 2\sqrt{\frac{b}{\pi\epsilon^2}} \int_0^\infty x \exp\left[-\frac{bx^2}{\epsilon^2}\right] dx = \sqrt{\frac{\epsilon^2}{\pi b}}. \tag{4.25}$$

Thus, the approximate rate function $\tilde{I}$ obtained from (4.20) is

$$\tilde{I}(\tilde{a}_b) = \frac{1}{2\epsilon^2} \int_0^\infty \left(F(x) - \tilde{F}_b(x)\right)^2 \tilde{p}_b(x)\, dx \tag{4.26}$$

$$= \frac{1}{\epsilon^2}\sqrt{\frac{b}{\pi\epsilon^2}} \int_0^\infty (bx - \gamma x)^2 \exp\left[-\frac{bx^2}{\epsilon^2}\right] dx, \tag{4.27}$$

which yields

$$\tilde{I}(\tilde{a}_b) = \frac{(b-\gamma)^2}{4b} \tag{4.28}$$

in terms of the parameter b. To obtain the approximation for that rate function in terms of a we use (4.25) to obtain

$$\tilde{I}(a) = \frac{\pi}{4}\left(\frac{\epsilon}{\pi a} - \frac{\gamma a}{\epsilon}\right)^2, \quad 0 < a < \sqrt{\epsilon^2/\pi\gamma} \tag{4.29}$$

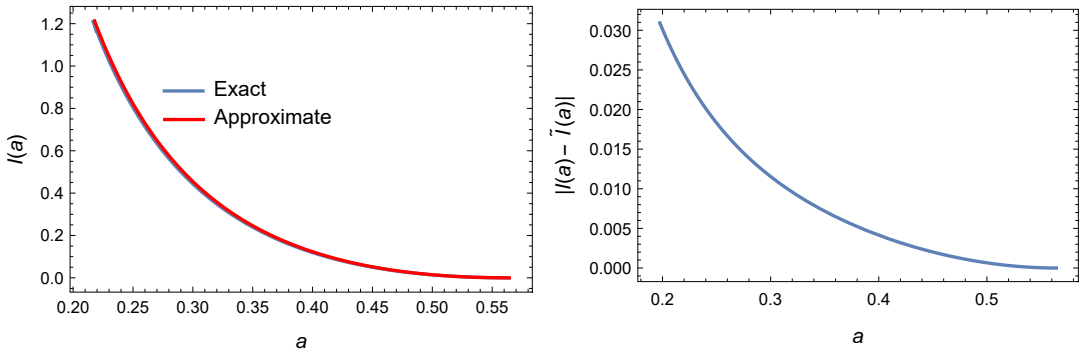

Figure 4.7: Comparison of the exact and approximate rate functions for $k < 0$ for the reflected Ornstein-Uhlenbeck process for the parameters $\epsilon = 1$ and $\gamma = 1$. Left: Plot of the exact and approximate rate functions. Right: Plot of the difference $|I(a) - \tilde{I}(a)|$.

and noting that $b > \gamma$ was assumed in our approximation.

This approximation is compared to the exact rate function in Fig. 4.7. We see that the approximation matches the zero a^*, as desired, since $b = \gamma$ recovers the force $F(x) = -\gamma x$. For $a < a^*$, the approximation is relatively good, with the approximation becoming worse as $a \to 0$. This can be understood from the behavior of F_k shown in Fig. 4.4. The driven force F_k has an increasingly negative value of $F_k'(0)$ as k decreases, and as x becomes large, we note that the driven force becomes linear with gradient $-\gamma$, the gradient of the original force $F(x)$. The greater the discrepancy between $F_k'(0)$ and $F'(0)$, the greater the curvature of the driven force has to be in order to have a linear gradient of $-\gamma$ for large x. This curvature is found mostly within a region close to $x = 0$, where p_k is concentrated. As k decreases, the greater the discrepancy between F_k and $\tilde{F}_{b(k)}$ will become in this region, given that the approximatate force has no curvature and is linear with gradient $-b(k) = F_k'(0)$. Given that this discrepancy between driven and approximate force occurs in a region where p_k is concentrated, the quality of the approximation will be affected negatively, and will decrease as k decreases, or equivalently as $a \to 0$.

We turn now to the approximation of the driven force for $k > 0$. Here the essence of the approximation will rely on the fact that the maximum value of $p_k(x)$ is no longer at $x = 0$ as for $k < 0$. In fact, as k increases so does the value $x^*(k)$ for which p_k is maximized, as can be seen from Fig. 4.6. This means that we want our approximate force $\tilde{F}$ to be a good fit of F_k close to $x^*(k)$. A simple approximate force that accomplishes this is

$$\tilde{F}_b(x) = -\gamma x + b, \quad b > 0. \tag{4.30}$$

This approximation relies on the fact that $x^*(k)$ lies in the region where F_k is essentially linear with slope $-\gamma$ with the parameter b controlling the value of the y-intercept of this linear function.

The potential $\tilde{U}_b$ corresponding to the force $\tilde{F}_b$ is given by

$$\tilde{U}_b(x) = \frac{\gamma}{2}\left(x - \frac{b}{\gamma}\right)^2. \tag{4.31}$$

As $\tilde{U}_b(x)$ is still quadratic, the stationary distribution $\tilde{p}_b$ is given by the shifted Gaussian

$$\tilde{p}_b(x) = \mathcal{N} \exp\left[-\frac{2\tilde{U}_b(x)}{\epsilon^2}\right] = \mathcal{N} \exp\left[-\frac{\gamma}{\epsilon^2}\left(x - \frac{b}{\gamma}\right)^2\right] \tag{4.32}$$

with normalization constant $\mathcal{N}$ given by

$$\frac{1}{\mathcal{N}} = \int_0^\infty \exp\left[-\frac{\gamma}{\epsilon^2}\left(x - \frac{b}{\gamma}\right)^2\right] dx = \frac{1 + \operatorname{erf}\left[\frac{b}{\epsilon\sqrt{\gamma}}\right]}{2}\sqrt{\frac{\pi\epsilon^2}{\gamma}}, \tag{4.33}$$

where we have introduced the error function $\operatorname{erf}(x)$ defined as

$$\operatorname{erf}(x) = \frac{2}{\sqrt{\pi}}\int_0^x e^{-z^2}\, dz, \tag{4.34}$$

so that $\tilde{p}_b$ is given by

$$\tilde{p}_b(x) = 2\sqrt{\frac{\gamma}{\pi\epsilon^2}}\frac{\exp\left[-\frac{\gamma}{\epsilon^2}\left(x - \frac{b}{\gamma}\right)^2\right]}{1 + \operatorname{erf}\left[\frac{b}{\epsilon\sqrt{\gamma}}\right]}. \tag{4.35}$$

The approximate $\tilde{a}_b$ is now obtained from (4.21) as

$$\tilde{a}_b = \int_0^\infty x\, \tilde{p}_b(x)\, dx = 2\sqrt{\frac{\gamma}{\pi\epsilon^2}}\frac{1}{1 + \operatorname{erf}\left[\frac{b}{\epsilon\sqrt{\gamma}}\right]}\int_0^\infty x \exp\left[-\frac{\gamma}{\epsilon^2}\left(x - \frac{b}{\gamma}\right)^2\right] dx. \tag{4.36}$$

Performing a change of variables $y = x - b/\gamma$ in the above integral yields

$$\tilde{a}_b = 2\sqrt{\frac{\gamma}{\pi\epsilon^2}}\frac{1}{1 + \operatorname{erf}\left[\frac{b}{\epsilon\sqrt{\gamma}}\right]}\int_{-\frac{b}{\gamma}}^\infty \left(y + \frac{b}{\gamma}\right) \exp\left[-\frac{\gamma}{\epsilon^2}y^2\right] dy. \tag{4.37}$$

We know from the calculation of the normalization constant appearing in $\tilde{p}_b$ that

$$\int_{-\frac{b}{\gamma}}^\infty \exp\left[-\frac{\gamma}{\epsilon^2}y^2\right] dx = \frac{1}{2}\sqrt{\frac{\pi\epsilon^2}{\gamma}}\left(1 + \operatorname{erf}\left[\frac{b}{\epsilon\sqrt{\gamma}}\right]\right) \tag{4.38}$$

since this is just the integral appearing in (4.33) with a change of variables. Finally, we have the antiderivative

$$\int ze^{-az^2}\, dz = -\frac{1}{2a}e^{-az^2} + C \tag{4.39}$$

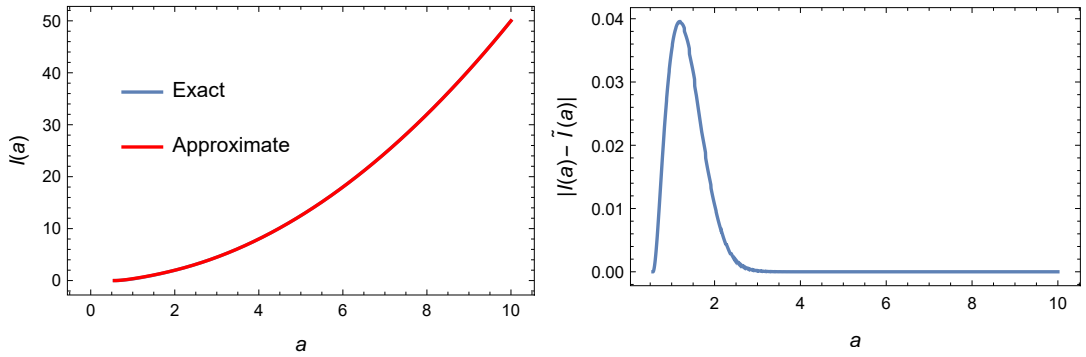

Figure 4.8: Comparison of the exact and approximate rate functions for $k > 0$ for the reflected Ornstein-Uhlenbeck process for the parameters $\epsilon = 1$ and $\gamma = 1$. Left: Plot of the exact and approximate rate functions. Right: Plot of the difference $|I(a) - \tilde{I}(a)|$.

so that

$$\int_{-\frac{b}{\gamma}}^{\infty} y \exp\left[-\frac{\gamma}{\epsilon^2}y^2\right] dy = \frac{\epsilon^2}{2\gamma} \exp\left[-\frac{b^2}{\gamma\epsilon^2}\right]. \tag{4.40}$$

Putting this all together yields

$$\tilde{a}_b = \sqrt{\frac{\epsilon^2}{\pi\gamma}} \frac{\exp\left[-\frac{b^2}{\gamma\epsilon^2}\right]}{1 + \operatorname{erf}\left[\frac{b}{\epsilon\sqrt{\gamma}}\right]} + \frac{b}{\gamma}. \tag{4.41}$$

From this result the approximate rate function $\tilde{I}$ is now obtained from (4.20) as

$$\tilde{I}(\tilde{a}_b) = \frac{1}{2\epsilon^2} \int_0^{\infty} \left(F(x) - \tilde{F}_b(x)\right)^2 \tilde{p}_b(x)\, dx = \frac{1}{2\epsilon^2} \int_0^{\infty} b^2\, \tilde{p}_b(x)\, dx = \frac{b^2}{2\epsilon^2} \tag{4.42}$$

as a function of the parameter b. Contrary to the $k < 0$ case, we cannot write the approximate rate function $\tilde{I}(\tilde{a}_b)$ as a function $\tilde{I}(a)$ of a only, since we cannot here write b explicitly in terms of $\tilde{a}_b$, as can be seen from the expression (4.41). We can still however plot the approximate rate function $\tilde{I}(\tilde{a}_b)$ parametrically.

The approximate and exact rate functions are compared in Fig. 4.8. The correspondence between these two functions is seen to be essentially exact, with a small range of values of $a > a^*$ for which the correspondence between the two functions breaks down, after which the correspondence becomes virtually exact. This breakdown in the approximation can be explained with reference to Fig. 4.6. We see that there is a small range of values of k for which the invariant distribution p_k is not of a Gaussian form, with the wave packet still attached to the boundary. For these values of k the linear approximation is not as appropriate as for those values of k for which the wave packet is (virtually) entirely free from the boundary and for which we observe from Fig. 4.8 that the linear approximation for F_k becomes almost exact.

While the expression (4.41) for $\tilde{a}_b$ seems complicated, we see that for increasing b (which corresponds to increasing k) $\tilde{a}_b$ becomes increasingly linear due to the decay of the exponential $\exp[-b^2/\gamma\epsilon^2]$. This, along with the quadratic form (in b) for $\tilde{I}$ obtained in (4.42) and the high degree of correspondence between the exact and approximate rate functions, implies that the fluctuations for $k > 0$ are essentially Gaussian. In other words, the rate function $I(a)$ is essentially parabolic for $a > a^*$.

4.2 Reflected Brownian Motion with Drift

We now turn our attention to the second application involving the reflected Brownian motion process with drift considered in Section 3.2.1. As noted there, the reflecting boundary condition is implemented by demanding that the densities p on which the Fokker-Planck operator $\mathcal{L}$ act satisfy $p'(0^+) = -2\mu\, p(0^+)/\epsilon^2$. The SDE under consideration is gradient with the associated potential $U(x) = \mu x$ and with the properly normalized Gibbs stationary density given by (3.18).

4.2.1 Spectral Problem for Linear Observable

As in Section 2.7.1 we are interested in studying the linear observable A_T given in (2.48). The tilted generator $\mathcal{L}_k$ associated with A_T is given by

$$\mathcal{L}_k = -\mu\frac{d}{dx} + \frac{\epsilon^2}{2}\frac{d^2}{dx^2} + kf \tag{4.43}$$

and is non-Hermitian.

Given that $U(x) = \mu x$ for this SDE, the symmetrized (Hermitian) operator $\mathcal{H}_k$ is given from (2.42) and (2.43) by

$$\mathcal{H}_k = \frac{\epsilon^2}{2}\frac{d^2}{dx^2} - \frac{\mu^2}{2\epsilon^2} + kx \tag{4.44}$$

with the SCGF $\lambda(k)$ for the functional A_T now found as the dominant eigenvalue in the spectral problem

$$\left[\frac{\epsilon^2}{2}\frac{d^2}{dx^2} - \frac{\mu^2}{2\epsilon^2} + kx\right]\psi_k^{(n)}(x) = \lambda_n(k)\,\psi_k^{(n)}(x), \tag{4.45}$$

where the reflecting boundary condition (3.49) at $x = 0$ for the eigenfunctions $\psi_k^{(n)}$ becomes

$$\psi_k^{(n)\prime}(0) = -\frac{\mu}{\epsilon^2}\psi_k^{(n)}(0) \tag{4.46}$$

given that the force is $F(x) = -\mu$. This is a Robin (mixed) boundary condition on the eigenfunction $\psi_k^{(n)}$. Furthermore the eigenfunctions $\psi_k^{(n)}$ must be square-integrable and therefore must satisfy the decay condition

$$\lim_{x\to\infty}\psi_k^{(n)}(x)^2 = 0. \tag{4.47}$$

Note that bound state solutions to the spectral problem (4.45) exist only for $k < 0$ since the potential

$$\mathcal{V}_k(x) = \mu^2/2\epsilon^2 - kx \tag{4.48}$$

is confining only for $k < 0$.

The solutions to the differential equation (4.45) come from the class of Airy functions, with the Airy functions of the first kind $\mathrm{Ai}(x)$ and the Airy functions of the second kind $\mathrm{Bi}(x)$ being linearly independent solutions to (4.45). The Airy functions of the second kind are excluded since they do not satisfy the decay condition (4.47) and therefore are not square-integrable. The relevant class of solutions are therefore the Airy functions of the first kind, with solutions to (4.45) having the form

$$\psi_k^{(n)}(x) = \mathrm{Ai}\left[\left(-\frac{\epsilon^2}{2k}\right)^{2/3}\left(-\frac{2kx}{\epsilon^2} + \frac{2\epsilon^2\lambda_n(k) + \mu^2}{\epsilon^4}\right)\right], \quad k < 0. \tag{4.49}$$

While the solutions (4.49) come from the correct class of functions, we have yet to apply the boundary condition (4.46) which selects only those solutions which constitute appropriate solutions to our spectral problem and allows us to find the eigenvalues $\lambda_n(k)$. Upon substituting (4.49) into the boundary condition (4.46) we obtain the transcendental equation

$$\left(-\frac{2k}{\epsilon^2}\right)^{1/3}\mathrm{Ai}'\left[\left(-\frac{\epsilon^2}{2k}\right)^{2/3}\frac{2\epsilon^2\lambda_n(k) + \mu^2}{\epsilon^4}\right] + \frac{\mu}{\epsilon^2}\,\mathrm{Ai}\left[\left(-\frac{\epsilon^2}{2k}\right)^{2/3}\frac{2\epsilon^2\lambda_n(k) + \mu^2}{\epsilon^4}\right] = 0 \tag{4.50}$$

which is satisfied by the eigenvalues $\lambda_n(k)$. As in the previous application, this means that the eigenvalues $\lambda_n(k)$ correspond to the zeroes of the function $h(\lambda)$ given by

$$h(\lambda) = \left(-\frac{2k}{\epsilon^2}\right)^{1/3}\mathrm{Ai}'\left[\left(-\frac{\epsilon^2}{2k}\right)^{2/3}\frac{2\epsilon^2\lambda + \mu^2}{\epsilon^4}\right] + \frac{\mu}{\epsilon^2}\,\mathrm{Ai}\left[\left(-\frac{\epsilon^2}{2k}\right)^{2/3}\frac{2\epsilon^2\lambda + \mu^2}{\epsilon^4}\right] \tag{4.51}$$

with the SCGF $\lambda(k)$, the dominant eigenvalue of $\mathcal{H}_k$, corresponding to the maximal zero of $h(\lambda)$. A plot of $h(\lambda)$ is shown in Fig. 4.9.

The procedure now is the same as for the reflected Ornstein-Uhlenbeck process: for a given choice of the parameters ϵ and μ, the value of the maximal zero of $h(\lambda)$ is obtained for various k which allows us to obtain $\lambda(k)$ via interpolation. The result of this procedure is shown in Fig. 4.10. We observe again that $\lambda(0) = 0$, as required from the definition of $\lambda(k)$. As stated previously, $\lambda(k)$ is defined only for $k < 0$, given that these are the only values of k for which bound state solutions to our spectral problem exist. As for the reflected Ornstein-Uhlenbeck process, we have that $\lambda'(-\infty) = 0$ given that the lower bound of A_T is 0 and so $\lambda(k)$ becomes asymptotically linear as $k \to -\infty$.

The rate function $I(a)$ is obtained as before from the Legendre transform of the SCGF. The result is shown in Fig. 4.11. We note that $I(a)$ is defined for

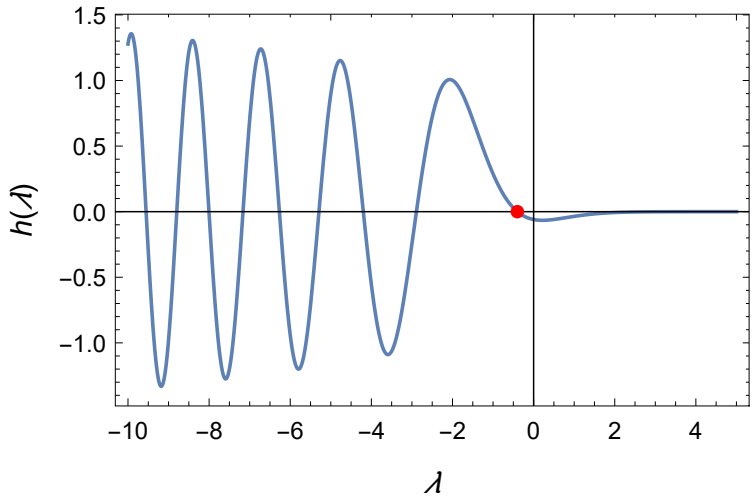

Figure 4.9: Function $h(\lambda)$ given by (4.51) for the parameter values $\epsilon = 1, \mu = 1$ and $k = -1$. Each zero represents an eigenvalue of the spectral problem (4.45). The red dot indicates the maximal eigenvalue for this set of parameters and therefore represents the SCGF for a specific value of k and a given set of parameters ϵ, μ.

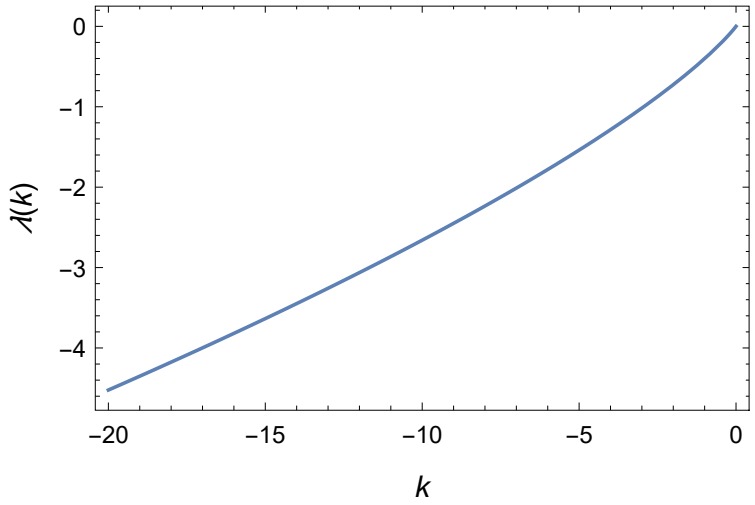

Figure 4.10: SCGF $\lambda(k)$ for the linear observable of reflected Brownian motion with drift for the parameter values $\epsilon = 1$ and $\mu = 1$.

$a \geq 0$, given that A_T is non-negative, and with $I(a)$ in principle also defined only up to $a^* = \lambda'(0)$, since $\lambda(k)$ is defined only for $k \leq 0$. The process under consideration is ergodic and so, as before, the zero a^* is found as the stationary expectation

$$a^* = \int_0^\infty x\, p^*(x)\, dx, \tag{4.52}$$

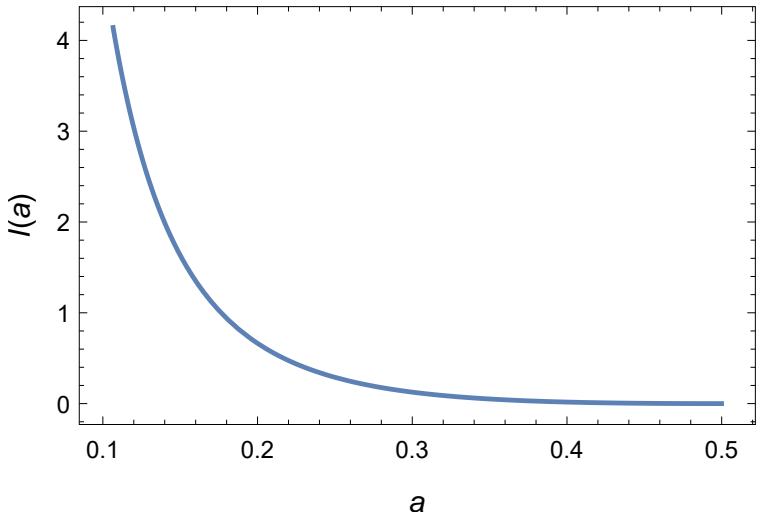

Figure 4.11: Rate function $I(a)$ for the linear observable of reflected Brownian motion with drift for the parameter values $\epsilon = 1$ and $\mu = 1$.

which, upon substituting (3.18) for p^* into the above equation, yields

$$a^* = \frac{2\mu}{\epsilon^2}\int_0^\infty x \exp\left[-\frac{2\mu x}{\epsilon^2}\right] dx = \frac{\epsilon^2}{2\mu}. \tag{4.53}$$

We note that the zero a^* is $1/2$ for the set of parameters $\epsilon = 1$ and $\mu = 1$, which is corroborated in Fig 4.11.

It is important to note at this point that A_T has fluctuations greater than a^*, but that these are not covered by the spectral calculation since $\lambda(k)$ is not defined for $k > 0$. For $a > a^*$, it is possible that $I(a) = 0$, indicating that the scaling of $p(A_T = a)$ for $a > a^*$ is weaker than exponential in T. Such a scaling was discussed recently by Nickelsen and Touchette [52] and is beyond the scope of this thesis.

To conclude this section, we derive the driven force F_k that realizes the fluctuation $a_k = \lambda'(k)$. Upon inserting the expression (4.49) for ψ_k into the expression (2.81) for the driven force F_k we obtain

$$F_k(x) = \epsilon^2\left(-\frac{2k}{\epsilon^2}\right)^{1/3} \frac{\mathrm{Ai}'\left[\left(-\frac{\epsilon^2}{2k}\right)^{2/3}\left\{-\frac{2kx}{\epsilon^2} + \frac{2\epsilon^2\lambda(k)+\mu^2}{\epsilon^4}\right\}\right]}{\mathrm{Ai}\left[\left(-\frac{\epsilon^2}{2k}\right)^{2/3}\left\{-\frac{2kx}{\epsilon^2} + \frac{2\epsilon^2\lambda(k)+\mu^2}{\epsilon^4}\right\}\right]}, \quad k < 0. \tag{4.54}$$

The driven force F_k is shown for different values of k in Fig. 4.12. We note that $F_k(0) = F(0) = -\mu$ for all k, as is expected following our discussion in Chapter 3. We also note that $x = 0$ is the only zero of the driven force F_k so that the maximum of the stationary density p_k will always be found at $x = 0$.

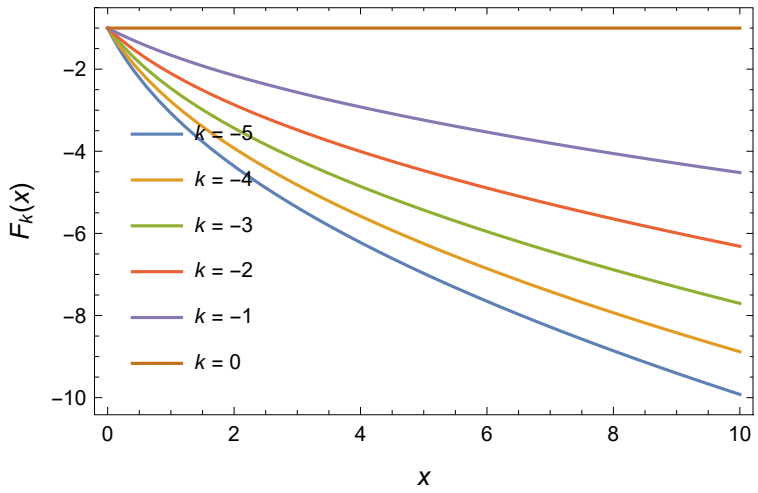

Figure 4.12: Driven force F_k for reflected Brownian motion with drift and with linear observable shown for various values of k for the choice of parameters $\epsilon = 1$, and $\mu = 1$.

4.2.2 Approximation of the Driven Process

As we did for the reflected Ornstein-Uhlenbeck process, we are now interested in modelling the driven force with a suitable approximation $\tilde{F}_b$ and in determining the accuracy of this approximation. The calculation here is simplified by the fact that we only have one case ($k < 0$) to consider, with the driven force F_k having qualitatively similar behavior for this range of values. In proceeding, we must choose an approximation $\tilde{F}_b$ that resembles the actual driven force F_k for those values of x for which the stationary density $p_k = \psi_k^2$ is maximized. We observe in Fig. 4.13 that the density p_k attains its maximum value at $x = 0$ after which it decays rapidly. This is the same as for the $k < 0$ case we encountered for the reflected Ornstein-Uhlenbeck process. We therefore use a linear approximation

$$\tilde{F}_b(x) = -bx - \mu, \quad b > 0 \tag{4.55}$$

as was done for the reflected Ornstein-Uhlenbeck process, with $b > 0$ since $F_k'(0) < 0$ for all values k under consideration, as is evident from Fig. 4.12. This linear approximation can be viewed as the first-order Taylor expansion of the true driven force, establishing a one-to-one relationship between k and b in the sense that, for every k, there exists a $b(k)$ such that $F_{b(k)}'(0) = F_k'(0)$. Furthermore, the $-\mu$ factor is included to ensure that $\tilde{F}_b(0) = -\mu$, as is the case for the true driven force.

The potential $\tilde{U}_b$ corresponding to the force $\tilde{F}_b$ is given by

$$\tilde{U}_b(x) = \frac{b}{2}\left(x + \frac{\mu}{b}\right)^2 \tag{4.56}$$

and satisfies $\tilde{U}_b'(x) = -\tilde{F}_b(x)$ as such a potential must. The invariant distribution

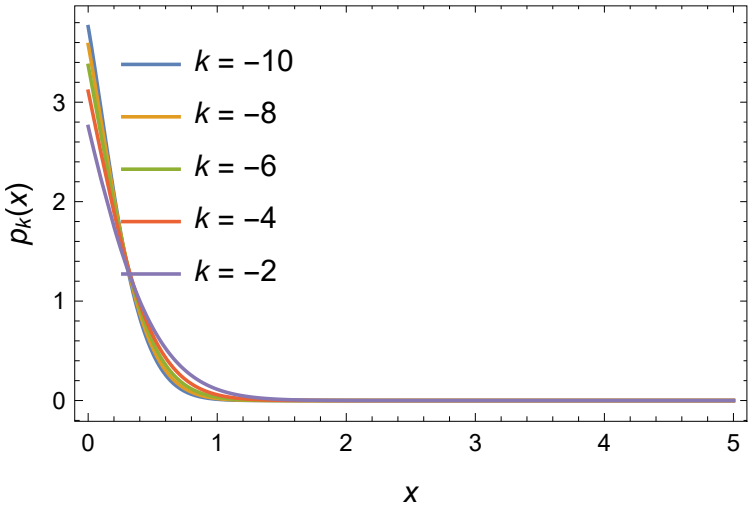

Figure 4.13: Invariant distribution p_k for reflected Brownian motion with drift and with linear observable shown for various values of k for the choice of parameters $\epsilon = 1$ and $\mu = 1$.

$\tilde{p}_b$ is found to be

$$\tilde{p}_b(x) = \mathcal{N} \exp\left[-\frac{2\tilde{U}_b(x)}{\epsilon^2}\right] = \mathcal{N} \exp\left[-\frac{b}{\epsilon^2}\left(x + \frac{\mu}{b}\right)^2\right] \tag{4.57}$$

with the normalization constant $\mathcal{N}$ satisfying

$$\frac{1}{\mathcal{N}} = \int_0^\infty \exp\left[-\frac{b}{\epsilon^2}\left(x + \frac{\mu}{b}\right)^2\right] dx = \frac{\epsilon}{\sqrt{b}}\left(\frac{\sqrt{\pi}}{2} - \frac{\sqrt{\pi}}{2}\operatorname{erf}\left[\frac{\mu}{\epsilon\sqrt{b}}\right]\right), \tag{4.58}$$

where we have used the definition of the error function (4.34). We therefore have that the properly normalized density $\tilde{p}_b$ is given by

$$\tilde{p}_b(x) = 2\sqrt{\frac{b}{\pi\epsilon^2}} \frac{\exp\left[-\frac{b}{\epsilon^2}\left(x + \frac{\mu}{b}\right)^2\right]}{1 - \operatorname{erf}\left[\frac{\mu}{\epsilon\sqrt{b}}\right]}. \tag{4.59}$$

We can now calculate the approximations $\tilde{a}_b$ and $\tilde{I}$ associated with the drift $\tilde{F}_b$. As before, we obtain $\tilde{a}_b$ from the relation (4.21) and $\tilde{I}$ from the relation (4.20). We have

$$\tilde{a}_b = \int_0^\infty x\, \tilde{p}_b(x)\, dx = 2\sqrt{\frac{b}{\pi\epsilon^2}} \frac{1}{1 - \operatorname{erf}\left[\frac{\mu}{\epsilon\sqrt{b}}\right]} \int_0^\infty x \exp\left[-\frac{b}{\epsilon^2}\left(x + \frac{\mu}{b}\right)^2\right] dx, \tag{4.60}$$

with the calculation proceeding in an identical manner as in (4.36) to (4.41), yielding the result

$$\tilde{a}_b = \sqrt{\frac{\epsilon^2}{\pi b}} \frac{\exp\left[-\frac{\mu^2}{\epsilon^2 b}\right]}{1 - \operatorname{erf}\left[\frac{\mu}{\epsilon\sqrt{b}}\right]} - \frac{\mu}{b}. \tag{4.61}$$

For the approximate rate function $\tilde{I}$ we have

$$\begin{aligned}\tilde{I}(\tilde{a}_b) &= \frac{1}{2\epsilon^2}\int_0^\infty \left(F(x) - \tilde{F}_b(x)\right)^2 \tilde{p}_b(x)\, dx \\ &= \frac{b^2}{\epsilon^2}\sqrt{\frac{b}{\pi\epsilon^2}} \frac{1}{1 - \operatorname{erf}\left[\frac{\mu}{\epsilon\sqrt{b}}\right]} \int_0^\infty x^2 \exp\left[-\frac{b}{\epsilon^2}\left(x + \frac{\mu}{b}\right)^2\right] dx. \end{aligned} \tag{4.62}$$

The integral is essentially the second moment of a shifted Gaussian that we evaluate as follows. Changing variables to $z = \frac{\sqrt{b}}{\epsilon}(x + \mu/b)$ in the integral yields

$$\tilde{I}(\tilde{a}_b) = \frac{b^2}{\epsilon^2}\sqrt{\frac{b}{\pi\epsilon^2}} \frac{1}{1 - \operatorname{erf}\left[\frac{\mu}{\epsilon\sqrt{b}}\right]} \frac{\epsilon}{\sqrt{b}} \int_{\frac{\mu}{\epsilon\sqrt{b}}}^\infty \left(\frac{\epsilon z}{\sqrt{b}} - \frac{\mu}{b}\right)^2 e^{-z^2}\, dz. \tag{4.63}$$

Now, we have

$$\begin{aligned}\int_{\frac{\mu}{\epsilon\sqrt{b}}}^\infty \left(\frac{\epsilon z}{\sqrt{b}} - \frac{\mu}{b}\right)^2 e^{-z^2}\, dz =& \frac{\epsilon^2}{b}\int_{\frac{\mu}{\epsilon\sqrt{b}}}^\infty z^2\, e^{-z^2}\, dz - \frac{2\epsilon\mu}{b^{3/2}}\int_{\frac{\mu}{\epsilon\sqrt{b}}}^\infty z\, e^{-z^2}\, dz \\ &+ \frac{\mu^2}{b^2}\int_{\frac{\mu}{\epsilon\sqrt{b}}}^\infty e^{-z^2}\, dz \end{aligned} \tag{4.64}$$

where from previous calculations we know that

$$\int_{\frac{\mu}{\epsilon\sqrt{b}}}^\infty z\, e^{-z^2}\, dz = \frac{1}{2}\exp\left[-\frac{\mu^2}{\epsilon^2 b}\right] \tag{4.65}$$

and

$$\int_{\frac{\mu}{\epsilon\sqrt{b}}}^\infty e^{-z^2}\, dz = \frac{\sqrt{\pi}}{2}\left(1 - \operatorname{erf}\left[\frac{\mu}{\epsilon\sqrt{b}}\right]\right). \tag{4.66}$$

As for the integral with integrand $z^2 e^{-z^2}$, we note the relationship

$$\int_c^\infty z^2\, e^{-z^2}\, dz = -\left[\frac{d}{da}\int_c^\infty e^{-az^2}\, dz\right]_{a=1}. \tag{4.67}$$

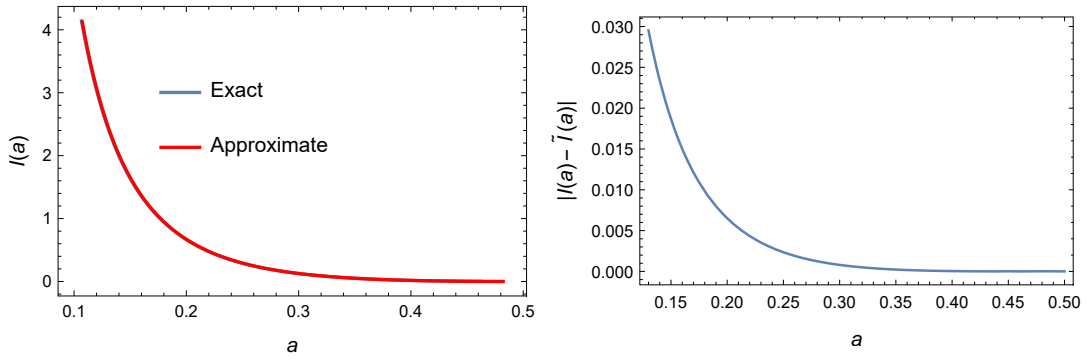

Figure 4.14: Comparison of the exact and approximate rate functions for $k < 0$ for reflected Brownian Motion with drift and linear observable for the parameters $\epsilon = 1$ and $\mu = 1$. Left: Plot of the exact and approximate rate functions. Right: Plot of the difference $|I(a) - \tilde{I}(a)|$.

We have

$$\begin{aligned}\frac{d}{da}\int_c^\infty e^{-az^2}\,dz &= \frac{d}{da}\frac{1}{\sqrt{a}}\int_{\sqrt{a}c}^\infty e^{-y^2}\,dy \\ &= \frac{\sqrt{\pi}}{2}\frac{d}{da}\left[\frac{1}{\sqrt{a}}\left(1-\operatorname{erf}\left(\sqrt{a}c\right)\right)\right] \\ &= \frac{\sqrt{\pi}}{2}\left[-\frac{1}{2a^{3/2}}\left(1-\operatorname{erf}\left(\sqrt{a}c\right)\right)-\operatorname{erf}'\left(\sqrt{a}c\right)\frac{d}{da}\left(\sqrt{a}c\right)\right] \\ &= -\frac{\sqrt{\pi}}{4a^{3/2}}\left(1-\operatorname{erf}\left(\sqrt{a}c\right)\right)-\frac{c}{2\sqrt{a}}e^{-ac^2} \qquad (4.68)\end{aligned}$$

where we have used

$$\frac{d}{dx}\operatorname{erf}(x) = \frac{2}{\sqrt{\pi}}e^{-x^2}. \qquad (4.69)$$

Upon substituting (4.68) into (4.67) we obtain

$$\int_c^\infty z^2\,e^{-z^2}\,dz = \frac{\sqrt{\pi}}{4}\left[1-\operatorname{erf}\left(\sqrt{a}c\right)\right]+\frac{c}{2}e^{-c^2}, \qquad (4.70)$$

such that

$$\int_{\frac{\mu}{\epsilon\sqrt{b}}}^\infty z^2\,e^{-z^2}\,dz = \frac{\sqrt{\pi}}{4}\left(1-\operatorname{erf}\left[\frac{\mu}{\epsilon\sqrt{b}}\right]\right)+\frac{\mu}{2\epsilon\sqrt{b}}\exp\left[-\frac{\mu^2}{\epsilon^2 b}\right]. \qquad (4.71)$$

Substituting (4.65), (4.66) and (4.71) into (4.64) and simplifying the resulting expression finally yields for the approximate rate function (4.63) the expression

$$\tilde{I}(\tilde{a}_b) = \left(\frac{b}{4}+\frac{\mu^2}{2\epsilon^2}\right)-\frac{\mu}{2}\sqrt{\frac{b}{\pi}}\frac{\exp\left[-\frac{\mu^2}{\epsilon^2 b}\right]}{1-\operatorname{erf}\left[\frac{\mu}{\epsilon\sqrt{b}}\right]} \qquad (4.72)$$

as a function of the parameter b. As before, we cannot eliminate the parameter b from the expression since the relation (4.60) cannot be inverted. However, we can plot the approximate rate function parametrically as $(\tilde{a}_b, \tilde{I}(\tilde{a}_b))$ by varying b. We note that

$$\lim_{b\to 0} \tilde{a}_b = \frac{\epsilon^2}{2\mu} = a^*, \tag{4.73}$$

and

$$\lim_{b\to 0} \tilde{I}(\tilde{a}_b) = 0, \tag{4.74}$$

such that the approximation matches the exact rate function for $b = 0$ or, equivalently, $k = 0$, as it must.

The exact and approximate rate functions are compared in Fig. 4.14. As can be seen, the correspondence between the functions are good, with the correspondence between the functions becoming increasingly exact as $k \to 0$ or $b \to 0$. The discrepancy between exact and approximate rate functions can be understood in much the same way as for the $k < 0$ case for the reflected Ornstein-Uhlenbeck process. As k decreases, the driven force has increasing curvature in a region where p_k is concentrated, while obtaining a linear gradient of 0 for large x. This means that as k decreases, the discrepancy between F_k and the linear $\tilde{F}_{b(k)}$ will increase in the region where p_k is concentrated. This accounts for the decreased fidelity of the approximation as $a \to 0$.

Chapter 5

Conclusions and Open Problems

We considered in this thesis the problem of determining the large deviations of a certain class of observables of Markov diffusions evolving in bounded domains. As a particular case, we considered one-dimensional (gradient) diffusions with reflecting boundary conditions to understand the manner in which the reflecting boundary condition is implemented in the spectral calculation associated with calculating the SCGF of a given observable.

In Chapter 2 we introduced the basic mathematical notions relating to stochastic differential equations and large deviations required for the calculations in the thesis. In particular, we introduced the SCGF and the spectral problem associated with it, as well as the notion of the driven process, which realizes, in the large time limit, given fluctuations of the observable.

Chapter 3 dealt with diffusions evolving in bounded domains, containing a general discussion of such diffusions before turning to one-dimensional diffusions with reflecting boundary conditions. Upon considering the large deviations of such diffusions, we obtained two important results.

Firstly, we defined the proper boundary condition for the spectral problem defining the SCGF when a perfectly reflecting boundary is present. This condition, as we have seen, is based on the fact that the large deviation operators $\mathcal{L}_k$ and $\mathcal{L}_k^\dagger$ are parameter extensions of the Markov generator $\mathcal{L}$ and its adjoint, the Fokker-Planck operator $\mathcal{L}^\dagger$, respectively. The operators $\mathcal{L}_k$ and $\mathcal{L}_k^\dagger$ therefore inherit the boundary conditions of $\mathcal{L}$ and $\mathcal{L}^\dagger$, respectively. Specifically, the tilted generator $\mathcal{L}_k$ inherits a Neumann boundary condition while its adjoint $\mathcal{L}_k^\dagger$ inherits the zero-current condition of the Fokker-Planck operator.

Secondly, the behavior of the driven process at a reflecting boundary is constrained by the boundary condition on the eigenfunctions of the operator $\mathcal{L}_k$, given that the driven force depends on the dominant eigenfunction r_k. In particular we found that the driven force and original force are equal at a reflecting boundary. This yields a zero current condition for the driven process at a reflecting boundary, which is natural considering that the driven process can be viewed as corresponding to the original process conditioned on realizing a given fluctuation in the long-time limit, so that the trajectories of the driven process

constitute a subset of the trajectories of the original process.

These results were illustrated in Chapter 4, where we obtained the large deviations of the area of the reflected Ornstein-Uhlenbeck process and reflected Brownian motion with negative drift and derived the driven processes associated with these large deviation problems. These applications allowed us to understand how reflecting boundaries change the large deviations compared to the case where no reflection is present. For Brownian motion with drift, no large deviations exist for the case where a reflecting boundary is not present, since this process has no stationary distribution. In this case the presence of a reflecting boundary has an important consequence for the existence of large deviations.

Furthermore, we found that for the systems considered, the driven process could be approximated in a very simple manner by using a linear approximation of the driven force near values of x for which the stationary distribution p_k of the driven process is maximized. This approximation allowed us to understand otherwise complicated driven processes through simple physical mechanisms.

We now indicate directions for further research. The first and most obvious direction is to consider which assumptions or restrictions were made in obtaining both our main conclusions and in the applications considered, and to weaken or modify these assumptions so as to consider applications from a more general class of processes. Specifically, we assumed that:

- The processes under consideration were one-dimensional, gradient and ergodic, with any boundaries being of the perfectly reflecting type.
- The observables under consideration were asumed to be of the form

$$A_T = \frac{1}{T}\int_0^T f(X_t)\,dt. \tag{5.1}$$

We conjecture that the framework developed in this thesis, which incorporates boundaries by viewing $\mathcal{L}_k$ and $\mathcal{L}_k^\dagger$ as parameter extensions, should hold true for processes taken from the more general classes of processes obtained by weakening the assumptions stated above to include, for example:

- Higher dimensional processes. In this case both the *type* and *geometry* of the boundary considered will be important. Additionally, stationary distributions in higher dimensions need not be of the Gibbs type. For reflecting boundaries in higher dimensions, with the boundary being smooth, the boundary condition on the Fokker-Plank operator becomes a zero-current condition in the direction normal to the boundary. It is an open problem to define or implement the reflecting boundary condition for non-smooth boundaries [15].
- Observables of the form

$$A_T = \frac{1}{T}\int_0^T f(X_t)\,dt + \frac{1}{T}\int_0^T g(X_t)\circ dX_t, \tag{5.2}$$

where g is not gradient. Such observables arise in the context of nonequilibrium processes [26]. In this case symmetrization might not be possible and the calculation of $\lambda(k)$ will be much more complicated, given that we now have to solve both the direct and adjoint spectral problems.

- Processes with multiplicative noise. A particularly interesting class of such processes is

$$dX_t = X_t(1 - X_t)\,dt + \epsilon X_t^{\alpha}\,dW_t, \quad 0 < \alpha \leq 1 \tag{5.3}$$

with $X_t \geq 0$ and absorbing boundary conditions at 0. The deterministic part of this SDE is known as a logistic growth model and has applications in biology in studies of population growth [53]. The effect of noise on the growth of a population is incorporated through the addition of the multiplicative noise term.

- Different types of boundaries. In particular, seeing what the implications for the driven force are in the case of sticky, elastic and absorbing boundary conditions (see definitions in Chapter 3).

To close, we note two open problems arising in the thesis. Typically, the operators $\mathcal{L}^{\dagger}$ and $\mathcal{L}$ are dual in the L^1/L^{∞} sense. In Chapter 2, we saw that, even for a process as simple as the Ornstein-Uhlenbeck process, the eigenfunctions of $\mathcal{L}_k^{\dagger}$ belong to L^1, while the eigenfunctions of $\mathcal{L}_k$ are not bounded and therefore do not belong to L^{∞}. A more in-depth understanding of the domains $\mathcal{D}(\mathcal{L}_k)$ and $\mathcal{D}(\mathcal{L}_k^{\dagger})$ is therefore required. Can we characterize the space that these eigenfunctions belong to?

Lastly, in considering the large deviations of the area of reflected Brownian motion with drift in Chapter 4, we were only able to obtain the large deviations for fluctuations a smaller than the typical value a^*, with the fluctuations $a > a^*$ not covered by the spectral calculation. Determining the large deviations for $a > a^*$ would complete our understanding of the fluctuations of this system and observable. This falls into the recent work done by Nickelsen and Touchette [52] on anomalous scaling of large deviations, for which no complete theory currently exists.

Bibliography

[1] K. Jacobs. *Stochastic Processes for Physicists: Understanding Noisy Systems*. Cambridge University Press, 2010.

[2] A. Einstein. Über die von der molekularkinetischen theorie der wärme geforderte bewegung von in ruhenden flüssigkeiten suspendierten teilchen. *Annalen der Physik*, 322(8):549–560, 1905.

[3] R. Newburgh, J. Peidle, and W. Rueckner. Einstein, Perrin, and the reality of atoms: 1905 revisited. *American Journal of Physics*, 74(6):478–481, 2006.

[4] M. Von Smoluchowski. Zur kinetischen theorie der brownschen molekularbewegung und der suspensionen. *Annalen der Physik*, 326(14):756–780, 1906.

[5] P. Langevin. Sur la théorie du mouvement brownien. *Compt. Rendus*, 146:530–533, 1908.

[6] H. Kunita. Itô's stochastic calculus: its surprising power for applications. *Stochastic Processes and their Applications*, 120(5):622–652, 2010.

[7] U. Seifert. Stochastic thermodynamics, fluctuation theorems and molecular machines. *Reports on Progress in Physics*, 75(12):126001, 2012.

[8] C. W. Gardiner. *Handbook of Stochastic Methods for Physics, Chemistry and the Natural Sciences*, volume 13 of *Springer Series in Synergetics*. Springer, New York, 2nd edition, 1985.

[9] K. Sekimoto. *Stochastic Energetics*. Springer, New York, 2010.

[10] R. Van Zon and E. G. D. Cohen. Stationary and transient work-fluctuation theorems for a dragged Brownian particle. *Physical Review E*, 67(4):046102, 2003.

[11] S. Meyn. *Control Techniques for Complex Networks*. Cambridge University Press, 2008.

[12] S. E. Shreve. *Stochastic Calculus for Finance II: Continuous-time Models*, volume 11. Springer, 2004.

[13] P. C. Bressloff. *Stochastic Processes in Cell Biology*. Springer, 2014.

[14] H. C. Berg. *Random Walks in Biology*. Princeton University Press, 1993.

[15] Z. Schuss. *Brownian Dynamics at Boundaries and Interfaces*. Springer, 2015.

[16] W. Feller. Diffusion processes in one dimension. *Transactions of the American Mathematical Society*, 77(1):1–31, 1954.

[17] W. Feller. The parabolic differential equations and the associated semigroups of transformations. *Annals of Mathematics*, 55:468–519, 1952.

[18] G. Peskir. On boundary behaviour of one-dimensional diffusions: From Brown to Feller and beyond. *William Feller-Selected Papers II. Springer, Berlin*, pages 77–93, 2015.

[19] N. Bou-Rabee and M. Holmes-Cerfon. Sticky Brownian motion and its numerical solution. *arXiv preprint: 1906.06803*, 2019.

[20] A. V. Skorokhod. Stochastic equations for diffusion processes in a bounded region. *Theory of Probability & Its Applications*, 6(3):264–274, 1961.

[21] A. V. Skorokhod. Stochastic equations for diffusion processes in a bounded region. II. *Theory of Probability & Its Applications*, 7(1):3–23, 1962.

[22] D. S. Grebenkov. NMR survey of reflected Brownian motion. *Reviews of Modern Physics*, 79(3):1077–1137, 2007.

[23] S. R. S. Varadhan. Asymptotic probabilities and differential equations. *Communications on Pure and Applied Mathematics*, 19(3):261–286, 1966.

[24] H. Touchette. The large deviation approach to statistical mechanics. *Physics Reports*, 478(1-3):1–69, 2009.

[25] A. Zeitouni and O. Dembo. *Large Deviations Techniques and Applications*. Springer-Verlag, New York, 1998.

[26] H. Touchette. Introduction to dynamical large deviations of Markov processes. *Physica A*, 504:5–19, 2018.

[27] R. Chetrite and H. Touchette. Nonequilibrium Markov processes conditioned on large deviations. *Annales Henri Poincaré*, 16(9):2005–2057, 2015.

[28] R. Chetrite and H. Touchette. Nonequilibrium microcanonical and canonical ensembles and their equivalence. *Physical Review Letters*, 111(12):120601, 2013.

[29] L. M. Ricciardi and L. Sacerdote. On the probability densities of an Ornstein-Uhlenbeck process with a reflecting boundary. *Journal of Applied Probability*, 24(2):355–369, 1987.

[30] A. R. Ward and P. W. Glynn. Properties of the reflected Ornstein-Uhlenbeck process. *Queueing Systems*, 44(2):109–123, 2003.

[31] W. H. Ha. *Applications of the reflected Ornstein-Uhlenbeck process*. PhD thesis, University of Pittsburgh, 2009.

[32] R. Chetrite and H. Touchette. Variational and optimal control representations of conditioned and driven processes. *J. Stat. Mech.*, 2015(12):P12001, 2015.

[33] M. D. Donsker and S. R. S. Varadhan. Asymptotic evaluation of certain Markov process expectations for large time, I. *Communications on Pure and Applied Mathematics*, 28(1):1–47, 1975.

[34] J. Gärtner. On large deviations from the invariant measure. *Theory of Probability & Its Applications*, 22(1):24–39, 1977.

[35] V. R. Fatalov. Brownian motion on $[0, \infty)$ with linear drift, reflected at zero: Exact asymptotics for ergodic means. *Sbornik: Math.*, 208(7):1014–1048, 2017.

[36] D. S. Grebenkov. Residence times and other functionals of reflected Brownian motion. *Physical Review E*, 76(4):041139, 2007.

[37] M. Forde, R. Kumar, and H. Zhang. Large deviations for the boundary local time of doubly reflected brownian motion. *Statistics & Probability Letters*, 96:262–268, 2015.

[38] R. Pinsky. The I-Function for diffusion processes with boundaries. *The Annals of Probability*, 13(3):676–692, 1985.

[39] R. Pinsky. A classification of diffusion processes with boundaries by their invariant measures. *The Annals of Probability*, 13(3):693–697, 1985.

[40] A. Budhiraja, P. Dupuis, et al. Large deviations for the emprirical measures of reflecting Brownian motion and related constrained processes in $\mathbb{R}_+$. *Electronic Journal of Probability*, 8, 2003.

[41] I. A. Ignatyuk, V. A. Malyshev, and V. V. Scherbakov. Boundary effects in large deviation problems. *Russian Mathematical Surveys*, 49:41–99, 1994.

[42] S. S. Sheu. A large deviation principle of reflecting diffusions. *Taiwanese Journal of Mathematics*, 2(2):251–256, 1998.

[43] P. Dupuis. Large deviations analysis of reflected diffusions and constrained stochastic approximation algorithms in convex sets. *Stochastics*, 21(1):63–96, 1987.

[44] L. Bo and T. Zhang. Large deviations for perturbed reflected diffusion processes. *Stochastics*, 81(6):531–543, 2009.

[45] F. Den Hollander. *Large Deviations*, volume 14 of *Fields Institute Monographs*. American Mathematical Society, 2008.

[46] G. R. Grimmett and D. Stirzaker. *Probability and Random Processes*. Oxford University Press, 3rd edition, 2001.

[47] H. Risken. *The Fokker-Planck Equation: Methods of Solution and Applications*. Springer, Berlin, 3rd edition, 1996.

[48] G. A. Pavliotis. *Stochastic Processes and Applications: Diffusion Processes, the Fokker-Planck and Langevin Equations*, volume 60. Springer, 2014.

[49] S. Karlin and H. E. Taylor. *A Second Course in Stochastic Processes*. Elsevier, 1981.

[50] P. E. Kloeden and E. Platen. *Numerical Solution of Stochastic Differential Equations*. Springer, 2013.

[51] R. Chetrite and H. Touchette. Variational and optimal control representations of conditioned and driven processes. *Journal of Statistical Mechanics: Theory and Experiment*, 2015(12):P12001, 2015.

[52] D. Nickelsen and H. Touchette. Anomalous scaling of dynamical large deviations. *Physical Review Letters*, 121(9):090602, 2018.

[53] L. J. S. Allen. *An Introduction to Stochastic Processes with Applications to Biology*. Chapman and Hall/CRC, 2010.